e-ISSN: 2791-8858
YIL/YEAR 2021
Cilt / Volume
1
Sayı/Issue 1
Eylül/ September

OMUJEST

OMU JOURNAL OF ENGINEERING SCIENCES AND TECHNOLOGY

ONDOKUZ MAYIS ÜNİVERSİTESİ
ONDOKUZ MAYIS UNIVERSITY

ONDOKUZ MAYIS ÜNİVERSİTESİ

MÜHENDİSLİK BİLİMLERİ VE TEKNOLOJİSİ DERGİSİ

ONDOKUZ MAYIS UNIVERSITY JOURNAL OF ENGINEERING SCIENCES AND TECHNOLOGY

e-ISSN: 2791-8858
Volume/Cilt: 1 Issue/Sayı: 1
Eylül/September 2021
Samsun

ONDOKUZ MAYIS ÜNİVERSİTESİ MÜHENDİSLİK BİLİMLERİ VE TEKNOLOJİSİ DERGİSİ
e-ISSN: 2791-8858
2021 Cilt: 1 Sayı: 1

OMU JOURNAL OF ENGINEERING SCIENCES AND TECHNOLOGY
e-ISSN: 2791-8858
2021 Volume: 1 Issue: 1

Ondokuz Mayıs Üniversitesi adına sahibi / Owner on behalf of Ondokuz Mayıs University
Prof. Dr. Yavuz ÜNAL
Rektör / Rector

Yönetici Editör / Managing Editor
Prof. Dr. Yıldıray TOPCU

Baş Editör / Editor-in-chief
Doç. Mevlüt GÜRBÜZ

Baş Editör Yardımcısı / Assistant Editor-in-chief
Prof. Dr. Mustafa AKTAŞ
Doç. Dr. Selim CEYLAN

Alan Editörleri / Section Editors
Prof. Dr. Arif Çağdaş AYDINOĞLU
Prof. Dr. Ahmet Hilmi ÇON
Prof. Dr. Okan ÖZGÖNENEL
Prof. Dr. Yüksel ARDALI
Doç. Dr. Özgür M. ARAZ
Doç. Dr. Sedat AKLEYLEK
Doç. Dr. Sedat DOĞAN
Doç. Dr. Selim CEYLAN
Doç. Dr. Sevim ALIŞIR
Dr. Öğr. Üye. Barış ÖZKAN
Dr. Öğr. Üye. Mahmut Can ŞENEL
Dr. Öğr. Üye. Mehmet Fatih YILMAZ
Dr. Öğr. Üye. Sedat YALÇINKAYA

Editör Yardımcıları / Associate Editors
Dr. Öğr. Üye. Sercan DEMİRCİ
Arş. Gör. Durmuş Özkan ŞAHİN
Arş. Gör. Fatih AYVENLİ
Arş. Gör. Hami SATILMIŞ
Arş. Gör. Onur YONTAR
Arş. Gör. Seyda ÖZBEKTAŞ
Arş. Gör. Zinnet Duygu AKŞEHİR

Mizanpaj / Layout
OMÜ Yayın Koordinatörlüğü

Grafik Tasarım / Graphic Design
Kısmet AYDIN
Sümeyye GÜMÜŞ UZUN
Fatma Hilal İÇİGEN
Cemre Aslan

Yayın Yeri ve Tarihi/Publication Place and Date
Samsun, 30 Eylül/September 2021

Ondokuz Mayıs Üniversitesi Mühendislik Bilimleri ve Teknolojisi Dergisi /OMU Journal of Engineering Sciences and Technology;
yılda iki kez yayımlanan hakemli bilimsel süreli bir yayın organıdır. Dergide yayınlanan yazıların her türlü içerik sorumluluğu yazarlara aittir. Yazılar; yayıncı kuruluşun izni olmadan kısmen veya tamamen bir başka yerde yayınlanamaz.

Yazışma Adresi / Corresponding Adress
Ondokuz Mayıs Üniversitesi Mühendislik Fakültesi (Dergi) Kurupelit / SAMSUN
Tel: +90 362 312 1919/1010

e-mail: jest@omu.edu.tr

İÇİNDEKİLER

OMÜ Mühendislik Bilimleri ve Teknolojisi Dergisi
OMU Journal of Engineering Sciences and Technology

e-ISSN: 2791-8858 OMU**JEST** September 2021, 1(1): 1-16

Influence of Tire Surface Geometry on Braking Performance of Aircraft Tires

Sefa YILMAZ[1], Aydemir Güralp URAL[2]

[1] Aerospace Engineering, Faculty of Aeronautics and Astronautics, Samsun University, Samsun, Turkey
•ssfylmz@gmail.com • ORCİD > 0000-0002-2258-4727

[2] Aerospace Engineering, Faculty of Aeronautics and Astronautics, Samsun University, Samsun, Turkey
• guralp.ural@samsun.edu.tr • ORCİD > 0000-0002-1178-7190

Makale Bilgisi / Article Information

Makale Türü / Article Types: Araştırma Makalesi / Research Article
Geliş Tarihi / Received: 23 Temmuz / July 2021
Kabul Tarihi / Accepted: 9 Eylül / September 2021
Yıl / Year: 2021 **| Cilt – Volume:** 1 **| Sayı – Issue:** 1 **| Sayfa / Pages:** 1-16

Atıf/Cite as: Atıf/Cite as: Yılmaz, S. ve Ural, A. G. "Influence of Tire Surface Geometry on Braking Performance of Aircraft Tires". Ondokuz Mayıs Üniversitesi Mühendislik Bilimleri ve Teknolojisi Dergisi - Ondokuz Mayis University Journal of Engineering Sciences and Technology, 1(1), September 2021: 1-16.

Sorumlu Yazar: Aydemir Güralp URAL

INFLUENCE OF TIRE SURFACE GEOMETRY ON BRAKING PERFORMANCE OF AIRCRAFT TIRES

ABSTRACT:

Almost half of the accidents in the last 20 years have occurred during landing phase of flight. Understanding the runway-tire contact mechanics of aircraft, is essential to prevent these accidents. There are several important parameters in the runway-tire interaction during landing. Among others, the footprint area, contact pressure area, vertical deflection of tire have the most influence on the landing performance of aircraft. To find out the effects of these parameters, commonly-held empirical equations have been used and even transformed into a user-friendly calculator VBA6 based on Visual Basic. Following this first part of theoretical calculations, the runway contact mechanics of aircraft tire is analyzed numerically by 3-D models of finite elements analyses (FEA). As a part of this comparative analyses, two substantially dissimilar tire models have been chosen with rib tread and cross tread surface patterns. Former model with rib tread is preferred for almost all civil aircrafts (i.e. ultra-light, light or passenger type), using airfields with tarmac or any other stabilized runway defined as soft landing field. But later cross tread pattern design is conceived for all terrain purposes and extensively used on airplanes regardless of vehicle size during World War II due to the lack of airfield conforming to aviation standards. In addition to our theoretical and numerical analyses, experimental results from literature has been used to complete the picture of runway-tire interaction during landing. Theoretical calculations show that rib tread pattern creates a non-linear relation by contrast to linearity on cross tread pattern between landing performance parameters such as footprint area, inflation pressure, vertical deflection. An increase in the aircraft vertical speed is observed corresponding to superior inflation pressure of tires as a result of higher nose angle. Similar correlation is made for vertical load on tire – it increases with vertical landing speed reduces due to the progressively higher nose angle during landing. Finite element (FE) analyses give more coherent results (3-8.5 %) with theoretical ones especially for footprint area. These numerical analyses obtained by different FE models ensure spatial and temporal details on the deformation of tires during landing, which enhance the comprehension of phenomena.

Keywords: *Braking performance; Predictive model; Surface geometry; Aircraft tire; Runway friction*

Highlights

- Evaluation of footprint area, contact pressure area and vertical deflection for landing performance.

- FE analyses on the behavior of different tire surface pattern on runway

INTRODUCTION

Due to the heavy air traffic and number of flight per airport, safe runway operations of modern aircraft have become more challenging because of higher landing and takeoff speeds, particularly under different runway conditions such as wet, slush or icy. Previous studies show that runway friction is significantly reduced under these conditions. In addition, some physical properties of tires have become more crucial than before such as surface geometry or tread pattern. Past studies have been performed to investigate the effect of various factors on the braking performance of aircraft tires under different runway conditions. These factors can be mainly listed into two groups, tire operational parameters (inflation pressure, load, speed), and runway conditions (water, snow, slush or any other surface contamination).

There are several studies on operational parameters of landing gears and aircraft tires. Behroozi et al. found that excellent precision in terms of deformation in finite element models. A fairly good estimation of tire burst pressure was obtained under high inflation, which is a risk for structural integrity during landing and even taxi [**1**]. Kizhakkethara showed that a non-linear analysis converges much easier if concentrated load is applied instead of pressure load and also produces better accuracy than with distributed load [**2**]. El-Shafei found that runway friction coefficient has a large effect on the contact pressure distribution; the inflation pressure has a considerable effect on the tire radial stiffness. Additionally, the study concludes that tire load carrying capacity is basically depends on the belt structure since the radial carcass ply has low stiffness in that direction [**3**]. Essienubong obtained that the higher the aircraft landing weight, the more damage aircraft tires undergo in terms of stress deformations and it builds up [**4**]. Cerezo et al. found that the correlation between weighted ground friction and braking coefficients is substantially greater relative to the correlation of unweighted coefficients [**5**].

When looking at studies on environmental as such runway conditions, there are some essential researches. Cerezo et al. observed in their model that the aircraft's successful slip ratio is expected to be surface-dependent, and values are calculated for each surface contaminants. The model curves of friction-slip and friction-speed are compared with experimental results. It has been found that the model is able to connect ground friction to aircraft braking efficiency with reasonable reliability [**6**]. Horne and Leland found that dry-runway friction coefficients are relatively insensitive to tire tread pattern. However, the magnitude of the friction coefficients developed by tires on contaminated runways was extremely sensitive to the tire tread pattern: circumferential-groove (or rib) treads developing the highest values of friction coefficient; where as smooth and dimple treads giving the lowest values for the investigated tread patterns and runway conditions [**7**]. Leland and Tay-

lor observed that a gradual degradation in braking effectiveness on the wet runway was experienced up to about 80% worn tire - tread condition; but the wet-runway friction coefficients dropped almost %50 and it's a remarkable decrease. Tires are completely worn out at the higher speeds, yet they continue to have about one-half the braking effectiveness of a new tire **[8]**. In another study, Joyner et al. showed that performance calculations are presented for a typical jet transport showing the effect of runway slush on the take-off distance; also shown are the effects of tire-to-runway braking coefficients on landing runout distances **[9]**. In their study, Pasindu et al. observed that the calibration and validation of the tire model, followed by computation of braking distances under different operating conditions of wheel load, tire inflation pressure, landing speed and water-film thickness **[10]**. Klein-Paste found a key result that aircrafts have experienced wet, snow covered runways more slippery than slush covered runways. The findings are there is no clear temperature dependency visible for contamination types **[11]**.

As a summary, in the literature it can be seen that finite element analyses and theoretical calculations on tire-pavement or tire-runway interaction under different terrain conditions, are present due to their affordable nature. Their binary combination becomes uncommon in the bibliography, and a comparative study with experimental data is even more rare. Behind that, high-cost, technology and expertise is required for experimental studies as most of aerospace research. As a solution, we combine results from our FE models, mathematical calculations in our study and experimental results of related research studies. This three-pillar (theoretical, numerical and experimental) aspect of our study provide more complete picture (i.e. global, spatial and temporal) of all phenomena took place during landing. It also explain the performance of aircraft tires on contact with runway and the effects of different surface patterns on tires.

MATERIALS AND METHODS

The methodology of the study can be seen in fig.1. Firstly some mathematical approaches are examined for determination essential parameters such as footprint area, contact pressure etc. Then these mathematical expressions are integrated to a calculator which is programmed on Visual Basic for Applications (VBA6). After doing that two different types of tires are created on Solidworks for making finite element analysis on ANSYS. Finite element analysis is made for two different models too. On the other hand an experimental research are determined to comparing results with each other. Finally all parameters are calculated with calculator and some comparisons were made with the FEA results and experimental results separately.

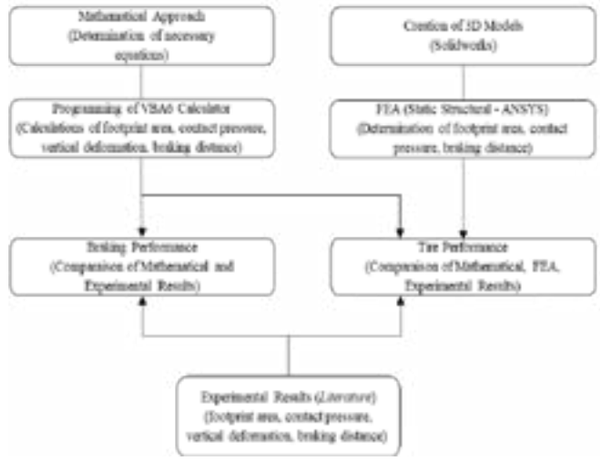

Figure 1. Methodology of study

Mathematical Approaches on Braking/Tire Performance

The calculator VBA6 is based on empirical equations accepted for the calculations of flight and landing performance of an aircraft. It uses also geometrical parameters of a real aircraft. In our case, this aircraft is Airbus A340-600. This calculator tool is programmed with Excel Visual Basic. Basically, it consists an excel file for calculating different parameters about braking performance of an aircraft during landing in the background; and a user-form with multiple tabs. Every tab calculates a parameter such as vertical deflection, footprint area or braking distance. When the user wants to calculate a parameter, all necessary data should be entered as input to the calculator.

The relationship between tire deflection, width and diameter, and vertical load and pressure is given by the following empirical formula in the Eq. (1) **[6]**:

$$Fz = (p_g + 0.08 \times p_r) \times w \times \sqrt{wd} \times 2.4 \times (\frac{\delta}{w} - c) \quad (1)$$

where Fz is vertical force, w is the tire width, d is tire diameter, p_g is inflation pressure, pr is rated inflation pressure, δ is deflection. c is an empirical coefficient.

The footprint area, A_p formula in the E_q. (2), is related to tire width and diameter **[12]:**

$$A_p = 2.3\sqrt{wd} \times (\frac{d}{2} - R_r) \quad (2)$$

Where R_r is rolling radius of the tire which can be calculated as $R_r = (\frac{d}{2} - \delta)$

The contact pressure, P_c in the in the Eq. (3) is given by following equation from Raymer **[12]:**

$$F_z = A_p \times P_c \qquad (3)$$

The total braking distance, S_{total} is calculated with the help of a set of equations. Each landing stages: approach, flare, free rolling and braking, are calculated separately. These stages can be seen in Fig. 2.

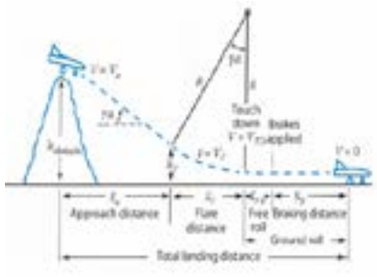

Figure 2. Landing stages of an aircraft **[12]**

The thrust, T (Eq. (4)) can vary with airspeed according to the rule

$$T = T_0\text{-a}V^2 \qquad (4)$$

where T_0 is thrust at zero airspeed (aka static thrust), T is thrust at airspeed V and a is a constant that can be positive, negative or null **[13]**. With this assumption, we can gather together coefficients of V^2 and terms that don't depend on V. It means that derivative of T with respect to time giving another equation. Also this equation has to be fit a format such as $T = \text{A-BV}^2$. Here, the A and B are two arbitrary parameters defined for braking stages (Eq. (5)) **[13]**.

$$A = g\,(\frac{T_0}{W} - \mu)$$

and

$$B = \frac{g}{w}[0.5\,\rho S\,(C_{D_g} - \mu C_{L_g}) + a] \qquad (5)$$

where W is weight, S wetted surface area, C_{D_g} and C_{L_g} are coefficients for ground level.

Also the coefficient K for induced drag parameter, should be recalculated for ground level as K_g **[13]**:

$K = \frac{q}{ARx\pi xe}$ and $K_g = \varphi K$, where AR is aspect ratio, e is Oswald efficiency factor.

Also the two approximations of the correction function φ is given by Eq. 6:

$$\varphi = 1 - \frac{2e}{\pi}\ln\,[1 + (\frac{\pi b}{8h})^2] \qquad (6)$$

where h_w is height of wing above the ground, b is wing span and e is Oswald efficiency factor **[13]**.

At this point, we have all the parameters we need in the equation, except for braking friction coefficient $\mu_{aircraft}$ (Eq. 7). Cerezo presented a suitable approach for the calculation of braking coefficient and by using it, the braking coefficient was evaluated **[6]**:

$$\mu_{aircraft} = \frac{\frac{T_r}{mg} - \frac{D}{mg} - \frac{\gamma}{g} - \epsilon}{1 - \frac{L}{mg}} \qquad (7)$$

T_r : Reverse thrust
D : Drag Force
L : Lift Force
ϵ : Runway Slope (typically %1.5)
γ : Deceleration
m : mass

Now all stages Sa, S_F, S_{FR}, S_B can be calculated separately by using following formulas (Eq. 8,9,10,11):

$S_a = \frac{h_{obstacle} - h_{TR}}{tan\Theta}$ Approach Stage (8)

$S_F = R\,sin\Theta$ Flare Stage (9)

$S_{FR} = \frac{1}{2B}\ln(\frac{A - B*V_{TD}^2}{A - B*V_B^2})$ Free Rolling Stage (10)

$S_B = \frac{1}{2B}\ln(\frac{A - B*V_B^2}{A})$ Braking Stage (11)

$S_{total} = S_a + S_F + S_{FR} + S_B$ Total Braking Distance (12)

By combining these different stages of landing, total braking distance S_{total} is obtained (Eq.12).

As a demonstration of The VBA6 visual interface and some input/output parameters, a screenshot of the calculator is shown in the Fig. A.1.

Finite Element Modelling

Our models includes basically three main parts: (1) tire, (2) rim and (3) runway. Before starting the analysis, boundary conditions and material information should be identified and set. The engineering data source in ANSYS software is mostly used when defining information about the properties of materials. Especially physical properties such as density, Poisson's ratio and yield strength etc. Aircraft tires for general use, are made of different layers of fibers and wires reinforcing rubber matrix. In the finite element model, if hyperelastic neoprene rubber in material database is selected alone for the tire, it is impossible for structure to bear the vertical force it is subjected to.

That is why, the model is simplified by the homogenization of the whole tire structure without distinct reinforcement parts but with embedded ones. Due to this homogenization process of the composite structure into an isotropic material, the tire properties will be slightly different than experimental results. Therefore, some important parameters such as density, yield strength were calculated with composite mixture law **[14]**. Firstly, percentage volumes and physical properties of typical tire components are determined (Table A.1 and Table A.2, respectively). Following that, the rule of mixture is applied with these values.

From the study of Dulanni and Kuruppu, tension test results of specimens made of real aircraft tire are used for the modulus of elasticity in the FE model **[15]**. Tension tests were made for a tire exposed to load of nearly 2,050 kg. The tire in our model is exposed to 22,500 kg. There is a great difference between these two tires. It is clear that pressure linearly changes with the vertical load until material gets yield. Also the modulus of elasticity should be proportional with the pressure which tire's surface is exposed to. If the two assumptions are interpreted together, it can be assumed that the modulus of elasticity is in a linear relationship with vertical load.

After the material information is defined, contact types were defined and mesh is created. There are two types of contact. One of them is bonded and ot-

her one is frictional. Bonded is between tire and rim. Frictional is between runway and tire with a coefficient 0.85, also there is no gap between tire and runway. Contact region adjusted to touch. So ANSYS is going to make an assumption like tire is touching to the runway. Here, during the mesh creation phase, some regions are set to high resolution mesh and other regions have comparatively less resolution. Especially, contact regions are adjusted to the high resolution for more precise calculation. After that, boundary conditions such as suspension force, inflation pressure, fixed support etc. are defined and the deformation analysis of the tire is completed (table 1). The details concerning mesh parameters are given in the table 2.

Table 1. Boundary Conditions of FE analysis

Boundary Conditions
Tire Inflation Pressure, p_g (1.184 MPa) **[16]**
Suspension Force (220,657 N)
Vertical Displacement, δ: (x- and y-axis are set to 0, z-axis is free)
Fixed Support
Standard Earth Gravity, g: 9.81 m²/s

Table 2. Mesh Parameters of FE analysis

Mesh parameters	
Mesh Elements	51,389
Mesh nodes	97,368
Average quality	0.71

Tire inflation pressure is calculated with mathematical method taken from Airbus HTPT report **[16]**.

RESULTS AND DISCUSSIONS

Footprint Area and Contact Pressure

Load on main gears in Airbus A340-600 is 180,000 kg. So a single main gear carry a weight of 90,000 kg. This load is for the strut distributing to four tires. Load acting on a single tire in main gear is 22,500 kg. Vertical directional force on the tire (F_z) is 22,500 × 9.807 = 220,657 N and p_g=11.84 bar and p_r=17.2 bar.

Recall the Eq. (1) so the vertical deflection δ is

$$\delta = 96.67 \text{ mm} = 9.67 \text{ cm}$$

Using this deformation value of δ due to the vertical forces, the contact area (footprint area) A_p can be calculated with Eq. (2)

$$A_p = 2.3\sqrt{53 \; x \; 140} \; x \; (\frac{140}{2} - (70\text{-}9.67)) = 1{,}915.83 \text{ cm}^2$$

This is the gross footprint area, the rib tread area should be subtracted from this value (fig. 3). When the tire has rib or cross pattern, the pattern area can be calculated with Solidworks software;

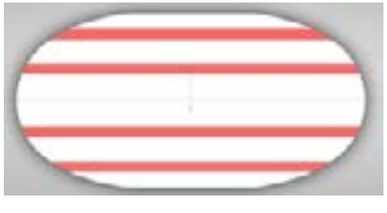

Figure 3. Representation of footprint area (white zone, in contact) of aircraft tire with rib tread (red zone, non-contact).

The sum of rib tread areas S_{rt} is:

$$S_{rt}=2\times(9087.45+11462.58)=41100\text{mm}^2= 411 \text{ cm}^2$$

The final footprint area A_p for rib tread tire is;

$$A_p = 1915.83 - 411 = 1504.83 \text{ cm}^2$$

Recall Eq. (3) for the contact pressure P_c

$$220{,}657=0.1505 \times P_c \text{ so } P_c=1.47 \text{ MPa}$$

These calculations are also made for the tire design with cross tread tire. The footprint area of cross tread tire are;

$$A_p = 1431.24 \text{ cm}^2 \text{ and } P_c=1.57 \text{ MPa}$$

Finite Element Analysis

As an example to a commercial aircraft landing gear, middle image is given (fig. 4 (b)). To this landing gear system, four wheels are attached but two front wheels and their tires are visible in this photograph. The surface geometry and tread texture of aircraft tires can be described as rib tread tires which is the type in our first FE model. Both in real life and the model, no thread are present on tire sidewalls. Tires are not deformed only in the vertical direction, but also in horizontal deformation. In our model appropriate to real life, the deformation are examined independently of the direction. In the rib tread model, if all nodes are accounted, the vertical deformation is in average 89.7 mm except some points around 120 mm.

Figure 4. Total Deformation of (a) rib tread tire (FEA), (b) actual tire on runway **[17]** and (c) cross tread tire (FEA), respectively.

If a similar FE analysis but with cross tread surface model, the vertical deformation is in average 61.1 mm but again some exception point of over 100 mm.

The total deformation of nodal distortion is the difference between their initial (non-contact) and final state (contact) positions of tire. Total deformations of rib tread and cross tread tires can be seen in the Fig. 4 (a) and (c). It is clear that cross tread is less deformed than rib tread.

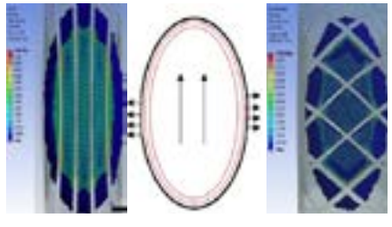

Figure 5. Contact Pressure Distribution of (a) rib-tread tire (FEA), (b) real tire (schematic representation) **[18]** and (c) cross tread (FEA), respectively

Actual pressure distribution on real tire-runway contact is represented at Fig. 5 (b). It belongs to measured ap-

parent contact related to BOEING test results [18]. The regions where the maximum pressure present are similar to the rib tread (Fig. 5 (a)). There is an increase of pressure up to 5.6 MPa on the edges of rib treads due to stress concentration which is the result of rib corner effect. This phenomenon reaches its highest peak for the outer ribs. On the other hand, the pressure diminishes less than 0.4 MPa near the center between ribs. Similar values are observed close to 0.4 MPa approaching the extremities of tire-runway contact area.

The pressure distribution for cross tread tire system is entirely different (Fig. 5 (c)). First there are a higher pressure distribution all around contact area, because the cross tread is less deformed. Another essential finding about cross tread is peak pressure. There are high pressure points of 12 MPa on the corners of tread crossing especially near the edge of contact area.

Comparison of Results

Some graphs were created through theoretical results such as vertical deflection, footprint area and braking distances with our VBA6 calculator. Subsequently, necessary comparisons were made between these parameters and their correlations are revealed. However, some other parameters such as inflation pressure is calculated manually with the output obtained by the calculator. Afterwards, braking distances on different runway conditions are shown vis-à-vis the values obtained by the calculator (Fig. A.2).

All these results are resumed in the Table 3, for comparison of parameters of footprint area A_p, contact pressure P_c and vertical deflection δ. In the table, it can be clearly seen that the FEA results approach the correct result in terms of many parameters except the contact pressure. This may be due to the simplification of the model and the use of linear elastic modulus. It is possible to say that many parameters such as elastic modulus, tensile yield strength, compressive yield strength are not constant due non-linear behavior in the real life.

One of the most important parameters to be examined is the amount of vertical deformation. The calculator's results and FEA results obtained should be compared with the Boeing experimental test results [8]. It is possible to say that the FEA result of the cross pattern is far from what is expected. Contrary to expectations, this does not affect the footprint area. When looking at the footprint area, the results are very consistent with each other especially for the rib pattern.

Table 3. Comparison of Results

Parameters	Tire Type	Mathematical Results	FEA Results	Boeing Test Results [18]
Footprint Area A_p (cm²)	Rib Tread (Gross)	1,915	-	1,840
	Rib Tread (Gross)	1,505	1,377	-
	Cross Tread (Gross)	1,915	-	-
	Cross Tread (Without Tread)	1,431	1,389	-
Contact Pressure P_c (MPa)	Rib Tread	1.47	1.14	1.53
	Cross Tread	1.57	1.01	-
Vertical Deflection δ (cm)	Rib Tread	9.67	8.97	9.7
	Cross Tread	9.67	6.11	-

It is possible to say that the vertical deformation and footprint area are in an almost linear relationship for cross pattern (Fig. 7). But the case with the rib pattern distinguishes from this linear relation especially when vertical deflection is higher than the values in the Fig. 6. When the Fig. 8 is examined, it can be understood that the growth rate of the footprint area slows down after a certain amount of vertical deformation for the rib pattern. In cross pattern, growth rate doesn't get slow but it increases constantly (Fig. 9).

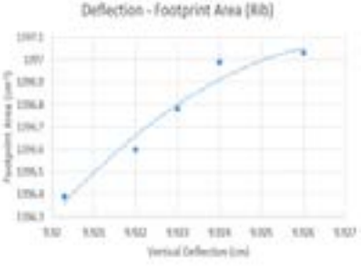

Figure 6. Vertical deflection versus footprint area for rib tread

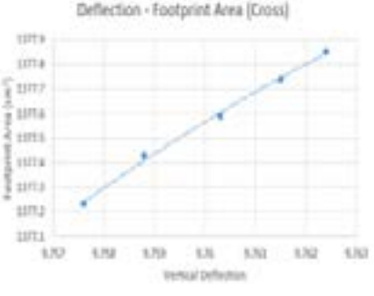

Figure 7. Vertical deflection versus footprint area for cross tread

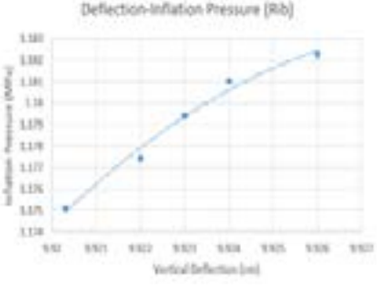

Figure 8. Vertical deflection versus inflation pressure for rib tread

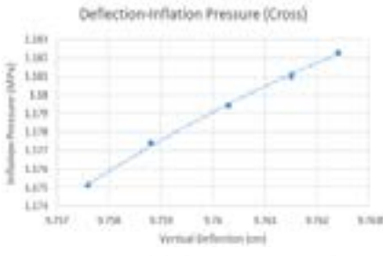

Figure 9. Vertical deflection versus inflation pressure for cross tread

As a regulation, almost 40% of airports throughout the world limit tire pressure of commercial aircrafts to 1.5 MPa. But today, new aircrafts have tire inflation pressures which can exceed this limit value [**18**]. One of the most important factors affecting the contact pressure is the inflation pressure. This parameter is directly related and delimiting factor to the durability or long-term performance of the material. Let's imagine two tires made of the same material but with different surface pattern, inflated at the same inflation pressure – the contact pressure of the tire with the cross pattern will be much higher than the rib pattern which becomes challenging in terms of material durability (Fig. 10).

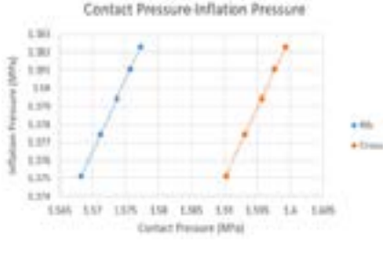

Figure 10. Contact pressure versus inflation pressure on tire

Additionally, static parameters are not the only reason why the cross pattern is not preferred in aircrafts. dynamic parameters are effective in this selection. The rib pattern performs better in phenomena such as runway friction coefficient, braking coefficient, hydroplaning. Another parameter to be examined is the vertical velocity at which the tire touches the ground. The speed of 2-4 m/s is accepted usually as a normal landing in ideal flight conditions. The speeds exceeding this limit are generally accepted as hard landing [**19**]. In the Fig. 11, the relationship between vertical landing speed and inflation pressure can be seen. It may seem that safe landing is approached when the vertical landing speed decreases, but this situation is actually quite complex. As the vertical landing speed decreases, the inflation pressure starts to increase. If the phenomena behind this situation is examined: when the aircraft touches the runway by increasing the nose angle to decrease the vertical touch speed, the load on the tire increases simultaneously. During this phenomenon, the amount of deformation and the footprint area should increase up to a certain point (Fig. 12). The footprint area is inversely proportional to the contact pressure, so the latter also augments. Finally, the inflation pressure increases related to the change of previous parameters. This chain reaction may seem very beneficial in terms of safety, but it should be noted that the tire may not be able to withstand all the load it is exposed structurally. There are factors such as sudden temperature increase caused by friction and shimmy, which adversely affect the structural properties of tires. For this reason, landing speed should be optimized and landing on the runway should be provided in the most appropriate way and braking should be done by taking into account the structural characteristics of aircraft tire.

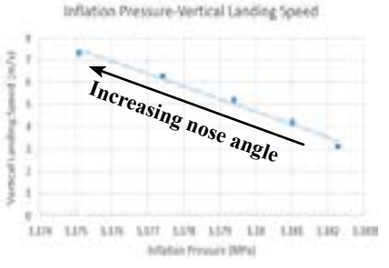

Figure 11. Inflation pressure versus vertical landing speed

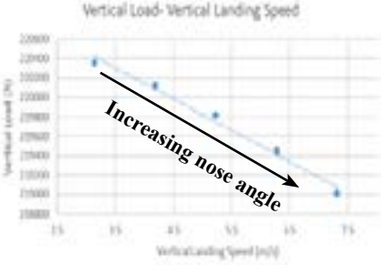

Figure 12. Vertical load versus vertical landing speed

CONCLUSION

This study presents comparative analyses between; theoretical results of a calculator tool VBA6 using well-accepted empirical equations for flight/landing performances and physical parameters of a specific aircraft; numerical results of finite element models for different surface pattern of tire like rib tread and cross tread. Finally, this comparative analyses are completed by experimental data from the literature. Footprint area, contact pressure and vertical deflection are the essential parameters used for these comparative analyses.

The analyses concludes on:

- footprint area, A_p- theoretical results gives good estimation of experimental behavior in the literature for rib tread pattern. Numerical FE and theoretical results are close to each other for both rib (8.5%) and cross (3%) tread patterns (tread area not included to A_p).
- contact pressure area, P_c- there is big coherency between mathematical and experimental values (4%) but a distinct difference between mathematical and FE results. It can be explained by the sensitive nature (spatially and temporally) of FE models compared to empirical equations in VBA6 calculator giving mostly only average values. Another reason for this difference, can be the simplification of some material (E, σ_y) and structural parameters (laminate structure).
- Vertical deflection, δ- this parameter gives total maximum displacement between initial and final states before and after the application of vertical load on tire by pavement (runway) or vice-versa. Theoretical results of VBA6 give much coherent values to experimental data. FE

numerical results are closer in rib tread pattern. The cross tread tire FE model give results relatively far from mathematical values. This situation is probably due to the aforementioned factors: simplification of tire structure and material properties, which are normally more complex.

- If all these parameters A_p, P_c, δ are correlated between each other and to other important criteria like inflation pressure, vertical landing speed (all parameters are VBA6 results in this analysis):

  footprint area and inflation pressure have a linear response to vertical deflection for cross tread tire pattern. These relations separate from linearity at higher vertical deflection both for inflation pressure and footprint area on rib tread tires. The vertical load on landing gear so on tires of the aircraft increases with vertical landing speed reduces due to the more and more higher nose angle during landing. A similar event happens in the relation of inflation pressure and vertical landing speed due to the change of nose angle while aircraft landing. More vertical speed is observed corresponding to superior inflation pressure of tires as a result of higher nose angle.

Appendices

Figure A.1. Calculator VBA6 based on Visual Basic

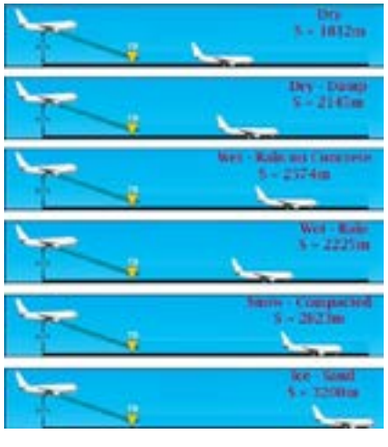

Figure A.2. Braking distances calculated for different runway conditions

TableA.1. Typical Tire Components Percentage Volumes [20]

Tire Components	Volume %
Rubber (natural or synthetic)	38
Filler (carbon black, silica, carbon chalk)	30
Reinforcement materials (steel belts)	16
Plasticizers	10
Chemicals	4
Anti-oxidants	1
Miscellaneous additives	1

Table A.2. New Material Properties According to Rule of Mixtures [14]

	Structural Steel as reinforcement (16%)	Neoprene Rubber (38%)	Composite Material for Tire (%100)
Density (kg/m^3)	7,850	1,250	1,731
Poisson's Ratio	0.3	0.45	0.219
Yield Strength (MPa)	250	-	40
Ultimate Strength (MPa)	460	-	73.6

Even tough chemical additives like plasticizers, anti-oxidants (Table A.1) change physical properties and as such mechanical performance of rubber in tire, they become neutral or ineffective in the rule of mixture. Only structural steel and neoprene rubber have high enough values to determine substantially the physical properties of new composite tire material (Table A.2). Therefore, in the calculation by the rule of mixture, respective values and volume percentage of structural steel and neoprene rubber are multiplied and added up to give a resultant value of total composite property (density, Poisson's ratio etc.) of aircraft tire.

REFERENCES

1. M. Behroozi, O.A Olatunbosun, W. Ding, "Finite Element Analysis of Aircraft Tyre – Effect of Model Complexity on Tire Performance Characteristics ", Materials Design, 35, ss. 810-819, 2012.

2. I. Kizhakkethara, "Non-Linear Static Analysis of Aircraft Tire Subjected to Inflation Pressure and Ground Contact Loads Using Finite Element Analysis", University of Calicut. India, 1991.

3. A.G. El-Shafei, H. Rothert, M.A. Barakat, "Nonlinear Three-Dimensional Finite Element Analysis of Contact Problem of Statically Loaded Tires", ss. 1-16, Sixth Cairo University, Cairo: International MDP Conference, 1996.

4. I.A. Essienubong, "Finite Element Analysis of Aircraft Tire Behaviour Under Overloaded Aircraft Landing Phase", Aeronautics and Aerospace Open Access, 2(1), ss. 35-39 [Online], available at: http://www.medcrave.com, 2018.

5. V. Cerezo, J. Gerthoffert, M. Bouteldja, "A Modeling-Based Approach to Relate Ground Friction Measurements to Aircraft Braking Performance", available at: http://arc.aiaa.org, 2015.

6. V. Cerezo, J. Gerthoffert, M. Bouteldja, "Modeling aircraft braking performance on wet and snow/ice-contaminated runways", Engineering Tribology, 00(00), ss.1-14 [Online], Available https://journals.sagepub.com/home/pij, 2015.

7. W.B. Horne, T.J.W Leland, "Influence of Tire

Tread Pattern and Runway Surface Condition n Braking Friction and Rolling Resistance of a Modern Aircraft Tire", NASA Technical Note TN D-1376, Langley Research Center, Hampton, 1962.

8. T.J.W. Leland, G.R. Taylor "An Investigation of the Influence of Aircraft Tire-Tread Wear on Wet-Runway Braking", NASA Technical Note, Langley Research Center, Hampton, 1965.

9. T.J. Upshur, W.B. Horne, T.J.W. Leland, "Investigations on the Ground Performance of Aircraft Relating to Wet Runway Braking and Slush Drag", NATO Report 429, Paris, France,1963.

10. H.R. Pasindu, T.F. Fwa, G.P. Ong, "Computation of Aircraft Braking Distances", Department of Civil Engineering National University of Singapore, Singapore, 2010.

11. A. Klein-Paste, "Airplane Braking Friction on Dry Snow, Wet Snow or Slush Contaminated Runways", Aerospace Science and Technology, 150, ss. 70-74 [Online], available at: http://www.elsevier.com, 2018.

12. D. P. Raymer, "Aircraft Design : A Conceptual Approach". 6th Edition. California: Conceptual Research Corporation, 2018.

13. L.R. Jenkinson, J.F. Marchman, "Aircraft Design Projects for Engineering Students", 1st ed., Elsevier Science Linacre House, Jordan Hill, Oxford, 2003.

14. W.D. Callister, "Materials Science and Engineering", 2nd ed. New York, NY, USA: Wiley, 2020.

15. K. A. Dulani. D. Kuruppu. "Case Study on Aircraft Tyre Wear in Y12 Aircraft Tyres", Royal Aeronautical Society, (01), ss. 10-12, 2018.

16. Airbus Airport Operations, "High Tire Pressure Test (HTPT)", ss. 17-18, Blagnac, France, 2010.

17. D.P. Fretwell, "Deformed Tire" available at: https://www.airliners.net/ (Accessed: April 2021).

18. O. Shepson, "Boeing and Airbus Tire Pressure Test Programs", ALACPA Airport Pavement Seminar and FAA Workshop, Sao Paulo, Brazil, 2009.

19. Aviation Safety Investigations & Reports, ATSB, "Hard Landing Involving an Airbus A330, 9M-MTA, Melbourne Airport, on 14 March 2015, Victoria", 2017.

20. G. Li, M. A. Stubblefield, G. Garrick, J. Eggers, C. Abadie and B. Huang, "Development of waste tire modified concrete", Cement and Concrete Research, vol. 34, 2283–2289, 2004.

OMÜ Mühendislik Bilimleri ve Teknolojisi Dergisi
OMU Journal of Engineering Sciences and Technology

e-ISSN: 2791-8858 OMU**JEST** September 2021, 1(1): 17-22

Pi Controller Design For Dcm Operated Boost Converter

Farzin ASADI[1]

[1] Department of Electrical and Electronics Engineering, Faculty of Engineering, Maltepe University, Istanbul, Turkey

• **farzinasadi@maltepe.edu.tr** • ORCID > 0000-0002-5928-0807

Makale Bilgisi / Article Information

Makale Türü / Article Types: Araştırma Makalesi / Research Article
Geliş Tarihi / Received: 9 Haziran / June 2021
Kabul Tarihi / Accepted: 15 Eylül / September 2021
Yıl / Year: 2021 **| Cilt – Volume:** 1 **| Sayı – Issue:** 1 **| Sayfa / Pages:** 17-22

Atıf/Cite as: Asadi, F. "Pi Controller Design For Dcm Operated Boost Converter". Ondokuz Mayıs Üniversitesi Mühendislik Bilimleri ve Teknolojisi Dergisi - Ondokuz Mayis University Journal of Engineering Sciences And Technology, 1(1), September 2021: 17-22.

PI CONTROLLER DESİGN FOR DCM OPERATED BOOST CONVERTER

ABSTRACT:

Controller design is an important phase of designing power electronics converters. Power electronics converters are non-linear dynamical systems. Without control output may not be what is needed by load. Power electronics converters are subject to disturbances like: input voltage's changes and/or output load's changes. Bypassing these disturbances and force the converter to track the reference command is the job of controller. This paper study the control problem of a boost converter operated in Discontinuous Conduction Mode (DCM). Instead of using well known linear model extraction techniques like State Space Averaging (SSA) or circuit averaging which requires a large amount of calculations and considerable amount of time to learn the methods itself, a system identification approach is used for modeling. A PI controller is designed for the obtained model. Close loop system is tested in Simulink® environment. Simulation results showed the performance of designed controller.

Keywords: *Boost converter; Discontinuous conduction mode; Feedback control; Non-minimum phase system; System identification*

INTRODUCTION

Power electronics converters require negative feedback to provide a suitable output voltage or current for the load. Although control engineering has considerable progress over recent decades, most applications use PID controllers, because of their low price and simplicity. Generally speaking, using derivative term is not so common in power electronics converters control. Usually a P or PI controller is all that is required. Designing a classical P or PI controller for a power electronics converter is started by obtaining the model of converter. Various techniques can be found in literature to obtain a Linear continuous Time Invariant (LTI) model of a DC-DC converter. The most well known methods are: Current injected approach, circuit averaging and state space averaging.

Table 1, is a general comparison between CCM and DCM in DC-DC converters.

Table 1. Comparison of CCM and DCM

Continuous Current Mode(CCM)	Discontinuous Current Mode(DCM)
	• Voltage gain is a function of load and design parameters
• Voltage gain is independent of load	• Input current is pulsating
• Input current is continuous and non pulsating	• Commutation of controlled switch is made with zero current which reduce commutation losses.
• Efficiency is higher in comparison with DCM	• Inductor size can be reduced drastically in comparison with CCM.

One important feature of boost converter is the Non-Minimum Phase (NMP) characteristic which is due to the Right Half Plane (RHP) zero in its control to output voltage transfer function. NMP effect deteriorates the control and stability behavior of the converter. DCM operation is an available alternative to CCM. In this case, the RHP zero places in high frequencies, usually higher than switching frequency and the boost converter mainly behaves like a converter with a single pole. Considering the disadvantage of DCM operation like high current ripple and low efficiency, in some special applications when control is important, power circuit designers intentionally design the controller to operate in DCM operation.

RELATED WORKS

Foundation of State Space Averaging (SSA) was laid down in Middlebrook RD et al. (1977). The first attempt to model Discontinuous Conduction Mode (DCM) is presented in. Cuk S et al. (1977). Accurate small signal models for DCM operation were developed by Sun J et al. (2001). The current injected method (Kislovski, et al (1991) and Mohan et al. (2003)) can do the job of modeling in either CCM or DCM. A unified SSA based method to develop both CCM and DCM was developed by Suntio T. (2006). Circuit averaging gained a lot of attention recently due to its generality (Hren A. et al.2005). A comprehensive survey of the modeling issues can be found in Maksimovic et al. (2001).

Application of different control methods to power electronics converters has been studied in many papers. For example, feedback linearization(-Sanders GC, et al. (1986)), sliding mode control (Sira-Ramirez H, et al. (1987)), PID control (Venkatanarayanan S, et al. (2014)) and H_∞ design(Rodriguez H, et al. (2005)) has been applied to Cuk converter, Linear Matrix Inequality(LMI) control has been applied to conventional boost by Kumar PR (2015). Discrete time controller has been designed for a boost converter in Alkrunz et al. (2016). A cascade state space controller is designed for buck mode of bidirectional dc-dc converter in Ocilka M, et al. (2010). PID control of SEPIC converter is studied in Veenalakshmi et al. (2014).

RESULTS AND DISCUSSIONS

Assume a boost converter with the following parameter values:

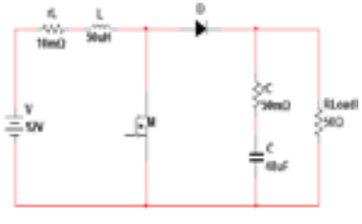

Figure 1. Boost converter used in simulations.

MOSFET M has on resistance of 100mΩ and diode D has forward voltage drop of 0.8 V and forward resistance of 1mΩ. Switching frequency is 25KHz.

Fig 2, shows the steady state inductor current:

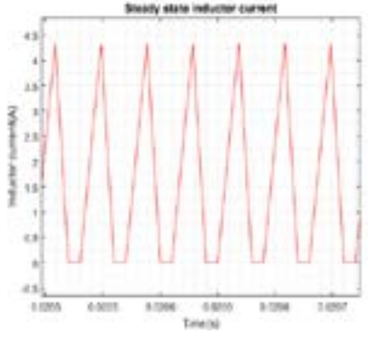

Figure 2. Steady state inductor current.

As shown in Fig. 2, inductor current returns to zero during each switching period. In order to obtain the small signal model around the given operating point, a small change is applied to the duty ratio and the corresponding output voltage is recorded. Fig. 3 and 4, shows the change in duty ration and output voltage, respectively.

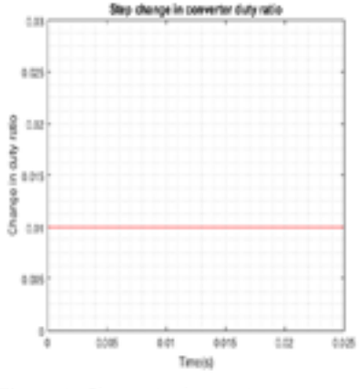

Figure 3. Change in duty ratio.

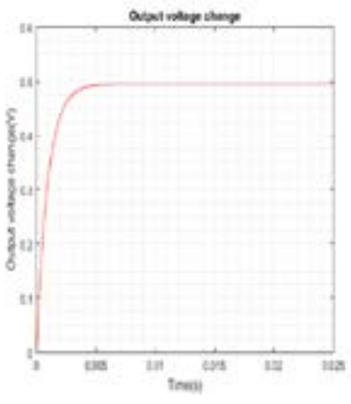

Figure 4. Change in output voltage.

System identification uses statistical methods to build mathematical models of dynamical systems from measured input-output data. Matlab® has a powerful system identification toolbox. It has a user friendly Graphical User Interface(GUI) which makes it easy to use. Using Matlab's system identification toolbox, following model is obtained for the input-output data shown in Fig. 3 and 4.

$$H(s) = \frac{-69240s + 4.085\ x\ 10^9}{s^2 + 78010s + 8.262\ x\ 10^7}$$

Control is done with a simple PI controller. Assume that phase margin of 80° and bandwidth of 500*Rad/s* is required. Using frequency domain design techniques (Ogata, 2003):

K_p=0.0066 and K_I=10.84

satisfy the given specifications.

SIMULATION RESULTS

Performance of designed controllers are tested with the aid of following scenario: Load resistance goes from R_{load}= 50Ω to R_{load}= 25Ω at t= 50ms, input source voltage changes from V_s= 12V to V_s= 18V at t=100ms and reference voltage has been changed from V_{ref}= 30V to V_{ref}= 40V at t=150ms. This scenario is summarized in Table 2:

Simulation results are shown in Fig.5.

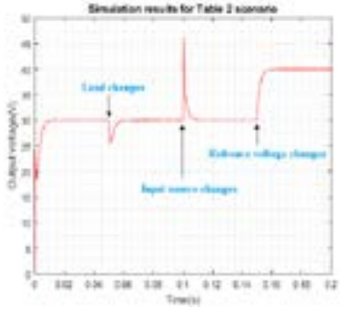

Figure 5. Simulation results.

Table 2. Test scenario

Parameter's name	Time	Initial value	Final value	(Final-Initial)/Initial
Rload	50 ms	50 Ω	25 Ω	-50%
V_s	100 ms	12 V	18 V	+50%
V_{ref}	150 ms	30 V	40 V	+33%

As seen in Fig. 5, output has zero steady state error. Controller keeps output voltage constant despite of changes in load resistance and input voltage.

CONCLUSION

Control theory plays an important role in power electronics. Providing a stable output voltage despite of changes in load and input voltage is not achievable without the use of control theory. Control problem of a boost convert operating in DCM studied in this paper. Instead of using complicated DCM mode modeling techniques, dynamical model of converter is extracted using system identification techniques. Controller is designed for the obtained model based on well known frequency response method. This procedure can be used for other type of converters operating in DCM.

REFERENCES

1. Alkrunz M, Yazıcı I(2016). Design of discrete time controller for the dc-dc boost converter. Sakarya university journal, vol. 4, pp.75-82.
2. Basso C(2008). Switch-Mode Power Supplies, McGraw-Hill, New York.
3. Cuk S and Middlebrook RD(1977). A general unified approach in modeling switching DC-to-DC converters in discontinuous conduction mode. in Proc. IEEE Power Electronics Special Conf. pp. 36–57.
4. Hren A, Slibar P(2005), Full order dynamic model of SEPIC converter, Proceedings of the IEEE International Symposium on Industrial Electronics, Dubrovnik, Croatia, vol. 2, pp. 553-558.
5. Kislovski A S, Ridl R and Socal N(1991). Dynamic

analysis of switching mode dc-dc converter, Van Nostrand Reinhold, New York.

6. Kumar PR, Kumar SG, Sandeep K. and Arun N(2015). LMI control of conventional boost converter. Indian journal of science and technology.Vol 8, pp50-52.

7. Maksimovic D, Stankovic AM, Tottuvelil VJ and Verghese GC(2001). Modeling and simulation of power electronic converters. Proc. IEEE, vol. 89, no. 6, pp. 898–912.

8. Middlebrook RD and Cuk S(1977). A general unified approach to modeling switching-converter power stages. Int. J. Electron., vol. 42, no. 6, pp. 521–550.

9. Mohan N, Undeland T and Robbins W(2003). Power electronics devices, converters appication and design, John Wiley and Sons, New York.

10. Ocilka M and BERES T(2010). State space controller for bidirectional dc-dc converter buck mode.Scientific conf. of young researchers, Kosice, Slovakia.

11. Ogata K(2003). Modern control engineering, Prentice Hall, New jersey.

12. Rodriguez H, Ortega R, Astolfi A(2005). Adaptive partial state feedback control of the DC-to-DC Cuk converter. Proceedings of the 2005 American Control Conference,Vol. 7, pp. 5121-5126.

13. Sanders GC, Verghese G and Cameron DF(1986). Nonlinear control laws for switching power converters. 25th IEEE conf. on decision and control.

14. Sira-Ramirez H, Ilic-Spong M(1987). Sliding motions on bilinear switched networks. IEEE Trans. on Circuits and Systems, CAS- 34(8): 919:933.

15. Sun J, Mitchell DM ,Greuel MF, Krein PT and Bass RM(2001). Average modeling of PWM converters in discontinuous modes. IEEE Trans. Power Electron., vol. 16, no. 4, pp. 482–492.

16. Suntio T(2006). Unified average and small-signal modeling of direct on-time control. IEEE Trans. Indust. Electron., vol. 53, no. 1, pp. 287–295.

17. Veenalakshmi S, Nedumal P and Selvaperumal(2014). Modeling and PID control of single switch bridgeless SEPIC PFC converter, Applied mechanics and materials, vol. 573, pp. 161-166.

18. Venkatanarayanan S and Saravanan M(2014). Research journal of applied science, engineering and technology.Vol. 8,no. 5, pp.623-629.

19. Venable D(1983). The K Factor: A New Mathematical Tool for Stability Analysis and Synthesis. Proceedings of 10th power con.

OMÜ Mühendislik Bilimleri ve Teknolojisi Dergisi
OMU Journal of Engineering Sciences and Technology

e-ISSN: 2791-8858 OMU**JEST** September 2021, 1(1): 23-31

Frekans Spektrum Doluluk Ölçümleri: OMÜ Kurupelit Yerleşkesi Örneği

Frequency Spectrum Occupancy Measurements: OMU Kurupelit Campus Example

Çetin KURNAZ[1], Eray ASLAN[2]

[1] Elektrik-Elektronik Mühendisliği Bölümü, Mühendislik Fakültesi, Ondokuz Mayıs Üniversitesi, Samsun, Türkiye
• **ckurnaz@omu.edu.tr** • ORCİD > 0000-0003-3436-899X

[2] Elektrik-Elektronik Mühendisliği Bölümü, Mühendislik Fakültesi, Ondokuz Mayıs Üniversitesi, Samsun, Türkiye
• **erayaslan93@hotmail.com** • ORCİD > 0000-0002-3709-1781

Makale Bilgisi / Article Information

Makale Türü / Article Types: Araştırma Makalesi / Research Article
Geliş Tarihi / Received: 28 Haziran / June 2021
Kabul Tarihi / Accepted: 27 Temmuz / July 2021
Yıl / Year: 2021 **| Cilt – Volume:** 1 **| Sayı – Issue:** 1 **| Sayfa / Pages:** 23-31

Atıf/Cite as: Kurnaz, Ç. ve Aslan, E. "Frekans Spektrum Doluluk Ölçümleri: OMÜ Kurupelit Yerleşkesi Örneği - Frequency Spectrum Occupancy Measurements: OMU Kurupelit Campus Example". Ondokuz Mayıs Üniversitesi Mühendislik Bilimleri ve Teknolojisi Dergisi - Ondokuz Mayis University Journal of Engineering Sciences And Technology, 1(1), September 2021: 23-31.

Sorumlu Yazar: Çetin KURNAZ

FREKANS SPEKTRUM DOLULUK ÖLÇÜMLERİ: OMÜ KURUPELİT YERLEŞKESİ ÖRNEĞİ

ÖZ:

Bu çalışmada, Ondokuz Mayıs Üniversitesi Kurupelit Yerleşkesinde baz istasyonlarını doğrudan gören sabit bir konumda, farklı gün ve saatlerde 50 MHz ile 2700 MHz arası frekans spektrumda ölçümler yapılarak spektrum doluluk oranları hesaplanmıştır. 4 saat aralıklarla ve 13 farklı zamanda yapılan spektrum ölçümlerinde RF-Explorer 6G Combo spektrum analizör kullanılmıştır. Spektrum ölçümlerinden baz istasyonlarının spektrum kullanım yoğunluklarının diğer servislere göre (örn. FM, TV) daha yoğun olduğu görülmüştür. Baz istasyonlarının spektrumlarının kullanım yoğunlukları -50 dBm, -60 dBm ve -70 dBm sinyali güç seviyeleri referans seçilecek analiz edilmiştir. Sonuçlardan spektrum doluluk oranlarının ölçüm zamanına, eşik sinyal güç seviyesine ve baz istasyonlarının kullandıkları servislere göre (GSM (2G), UMTS (3G), LTE (4G)) değiştiği görülmüştür. Ölçümlerde en yüksek spektrum yoğunluğu %100 ile LTE900 (-70 dBm için) için, en düşük spektrum yoğunluğu ise %0 ile LTE2600 (-50/-60 dBm için) hesaplanmıştır.

Anahtar Kelimeler: *Baz istasyonu; Frekans spektrum ölçümü; Frekans spektrum doluluk oranı; Bilişsel radyo.*

FREQUENCY SPECTRUM OCCUPANCY MEASUREMENTS: OMU KURUPELIT CAMPUS EXAMPLE

ABSTRACT:

In this study, frequency spectrum occupancy rates were determined using spectrum measurements results were obtained at different days and hours at a location where has line of sight with base stations in the Kurupelit Campus of Ondokuz Mayıs University in the frequency between 50 MHz and 2700 MHz. The measurements were performed using RF Explorer 6G Combo spectrum analyzer at 4-hour intervals and at 13 different times. It has been seen from the spectrum measurements that the spectrum occupancy rates of the base stations are much more than the other services (e.g., FM, TV). The spectrum occupancy rates of the base stations were analyzed for -50 dBm, -60 dBm and -70 dBm threshold values. From the results, it was seen that the spectrum occupancy rates changed according to the measurement time, the signal threshold level and the services used by the base stations (GSM (2G), UMTS (3G), LTE (4G)). In the measurements, the highest spectrum occupancy rate was calculated for LTE900 (for -70 dBm) with 100%, and the lowest spectrum occupancy rate was calculated for LTE2600 (for -50/-60 dBm) with 0%.

Keywords: *Base station; Frequency spectrum measurement; Frequency spectrum occupancy rate; Cognitive radio.*

Öne çıkanlar

- 50 MHz- 2700 MHz arası frekans spektrum ölçümleri.
- Baz istasyonu spektrum doluluk oranlarının hesaplanması.
- Spektrum doluluk oranının zamana ve eşik sinyal seviyesine göre değişiminin incelenmesi.

GİRİŞ

Teknolojik gelişmelerin bir sonucu olarak kablosuz iletişim sektöründe sunulan hizmetlerin sayısı her geçen gün artmaktadır. Artan kullanıcı taleplerini karşılayabilmek adına hücresel sistemlerin ve dolayısıyla hücresel sistemlerin temel yapı taşı olan baz istasyonların sayısı da artmaktadır. Her bir baz istasyonun sınırlı bir coğrafi bölgeye sınırlı bir frekans bandında hizmet vermektedir. Ülkemizde halihazırda üç farklı hücresel sistem teknolojisi kullanılmaktadır. Bunlar 2G (second generation) 3G (third generation) ve 4G (fourth generation)'dir. 2G (Global System for Mobile Communications, GSM) teknoloji genel olarak ses ve mesaj iletimi üzerine kurulmuş olup bu teknolojiyi kullanan baz istasyonları 900 MHz ile 1800 MHz frekans bantlarında çalışmaktadırlar. 2100 MHz frekans bantlarını kullanan 3G (Universal Mobile Telecommunication Service, UMTS) baz istasyonları saniyede 2 Mbit veri hızlarına olanak tanımaktadır. Bir 3G teknolojisi olan DC-HSDPA (Dual Carrier High-Speed Downlink Packet Access) ile bu veri hızı 42 Mbit'e kadar çıkabilmektedir. Spektrumda farklı frekans bantlarını kullanabilen (örn. 800 MHz, 2600 MHz) 4G (Long Term Evolution, LTE) teknolojisi ile veri hızları 100 Mbit/s kadar çıkabilmektedir. Ülkemizde üç farklı hücresel sistem operatörü (Turkcell, Vodafone ve Türk Telekom) bulunmakta olup her biri kendilerine ayrılan frekans bantlarında bu üç servis (2G, 3G ve 4G) hizmetini de vermektedirler.

Sınırlı bir kaynak olan frekans spektrumunu en yüksek verimde kullanmak her geçen gün daha fazla bir zorunluluk haline gelmektedir. Verimsiz ve statik frekans spektrumu kullanımının önüne geçmek adına dinamik spektrum yöntemi ilk olarak Mitola tarafından 1999 yılında ortaya atılmıştır [1]. Bilişsel radyo (cognitive radio) olarak adlandırılan bu kavram ile spektrumda yerleşen birincil kullanıcıların aldıkları hizmet kalitesinde bir düşüş yaşanmadan mevcut spektrumun dinamik olarak sezilmesi ve boş veya düşük güçlü frekans bantlarının kullanılması amaçlanmaktadır [2]. Kullanım oranı düşük spektrum bantlarının bilişsel radyo kablosuz haberleşme sistemleri tarafından kullanılması, spektrum yetersizliği problemi için umut verici bir çözüm olarak görülmektedir.

Bilişsel radyo uygulamaları günümüzün güncel çalışma konularından olup özellikle bilişsel radyo uygulamaları için frekans spektrumu ölçümleri üzerine literatürde yapılan pek çok çalışma bulunmaktadır. Bu çalışmalardan bazıları şu şekildedir. Samsun ili ve ilçelerini kapsayan 73 farklı konumda konumunda 470 MHz – 790MHz frekans aralığında spektrum doluluk ölçümleri yapılmıştır [3]. Samsun şehir merkezine TV vericilerini gören 10 farklı ko-

numda 470 MHz – 790MHz frekans bandında ölçümler yapılarak spektrum yoğunluğunun zamansal değişimi incelenmiştir [4]. Samsun şehir merkezinde 470 MHz – 790 MHz frekans aralığında, spektrumun en yoğun olduğu bölgede, 7 farklı günde ve 14 farklı zamanda spektrum doluluk ölçümleri yapılmıştır [5]. Samsun şehir merkezinde, 115 farklı konumda GSM900, LTE800, LTE900, GSM1800, LTE1800, UMTS2100 ve LTE2600 bantlarındaki spektrum doluluk ölçümleri yapılmıştır [6]. Kosova Cumhuriyetinin başkenti olan Priştina'da VHF (174 – 230 MHz) ve UHF bantlarında (470-860 MHz) spektrum ölçümleri yapılarak ile frekans spektrumlarının kullanım yoğunlukları analiz edilmiştir [7]. 174 MHz ile 1000 MHz arasındaki frekans bandı uzun süreli olarak izlenerek spektrum boşlukları belirlenmiştir [8]. Konya Selçuk Üniversitesi yerleşkesinde frekans spektrum ölçümleri 30 MHz – 3000 MHz arasında yapılmış ve Bilişsel Radyo uygulamaları için değerlendirmelerde bulunulmuştur [9]. Güney Afrika'da UHF, GSM900 MHz ve GSM1800 MHz bantlarında spektrum doluluk ölçümleri yapılmıştır [10]. Çin'in başkenti Pekin'de 450 MHz – 2700 MHz frekans aralığında 24 saat süreli spektrum doluluk ölçümleri yapılmıştır [11]. Samsun'da bina dışı ortamlarda GSM900 bandında spektrum doluluk değerlendirmeleri -40 dBm eşik seviyesi için yapılmıştır [12]. Ayrıca bilişsel radyonun evrimi [13] ve son yıllardaki güncel uygulamaları üzerine literatürde yapılan güncel pek çok çalışma bulunmaktadır [14-16].

Bu çalışmada, Ondokuz Mayıs Üniversitesi Kurupelit Yerleşkesinde spektrumun en yoğun olduğu bölgede 13 farklı zamanda spektrum ölçümleri yapılmıştır. 50 MHz – 2700 MHz arasındaki frekans spektrumu RF Explorer 6G Combo spektrum analizör [17] kullanılarak kayıt altına alınmıştır. Ölçüm sonuçları analiz edilerek frekans spektrumu doluluk oranları hesaplanmıştır. Hesaplanan spektrum doluluk oranlarının zamana, seçilen eşik seviyesine ve frekans spektrumunu kullanan servislere göre değişimleri incelenmiştir.

Makalenin geri kalanı şu şekilde organize edilmiştir: 2. Bölümde frekans spektrum ölçümlerin alınmasına yönelik materyal ve yöntem bilgileri ile spektrum doluluk oranı hesaplamaları verilmiştir. 3. Bölümde 50 MHz – 2700 MHz arasında yapılan spektrum ölçüm sonuçları ve spektrum doluluk oranları verilerek değerlendirmeler yapılmıştır. Makale 4. Bölüm olan Sonuçlar bölümü ile sonlandırılmıştır.

MATERYAL VE YÖNTEMLER

Bu çalışmada spektrum ölçümleri 6 Aralık 2018 16:00'da başlanılmış ve 12 Aralık 2018 saat 16:00'da sonlandırılmıştır. Ölçüm tarihleri ve saatlerine ait bilgiler Tablo 1'de verilmiştir. Ölçümlerde 15 MHz- 2700 MHz ve 4850 MHz- 6100 MHz arası frekansları ölçebilen RF Explorer 6G Combo spektrum analizör kullanılmıştır. RF Explorer 6G Combo'nun frekans çözünürlüğü 1kHz olup ortalama gürültü seviyesi -105 dBm'dir. Ölçümler OMÜ Kurupelit Kampüsünde baz istasyonu kaynaklı

Şekil 1. Frekans Spektrum ölçüm konumu ve ölçümlerin alınması

sinyal seviyelerinin en yüksek olduğu konumda yapılmıştır. Ölçümlerin alındığı konum ve örnek bir ölçüm ekran görüntüsü Şekil 1'de verilmiştir.

Tablo 1. Spektrum ölçüm tarih ve saatleri

Ölçüm Zamanı İndeksi	Ölçüm Tarihi	Ölçüm Saati
1	06.12.2018	16:00
2	06.12.2018	20:00
3	07.12.2018	00:00
4	07.12.2018	04:00
5	07.12.2018	08:00
6	07.12.2018	12:00
7	07.12.2018	16:00
8	07.12.2018	20:00
9	08.12:2018	00:00
10	08.12:2018	04:00
11	08.12:2018	08:00
12	08.12:2018	12:00
13	08.12:2018	16:00

Spektrum Doluluk Oranının Hesaplanması:

Bu çalışmada spektrum doluluk değerlendirmeleri Şekil 2'de verilenler çerçevesinde yapılmıştır. Spektrum doluluk incelemesi yapılacak frekans bandı M örnekten (örn. f_1, f_2, f_M) oluşmaktadır. Her bir frekans örneğinin ise gücü P (örn. P_1, P_2, P_M) ile ifade edilmektedir. Pθ ise sinyal gücü için eşik seviyesidir. Belirli bir frekanstaki sinyalin gücü eşik seviyesinden yüksek ise "1" aksi halde "0" olarak (1) eşitliğinde verildiği gibi ifade edilebilir.

$$\Delta(n) = \begin{cases} 0, & P_n < P\theta \\ 1, & P_n \geq P\theta \end{cases}, \quad n = 1,2,\ldots,M$$

Spektrum doluluk oranı (SDO) yüzdelik olarak (2) eşitliğinde verildiği gibi hesaplanır.

$$SDO = 100\ X\ \frac{\sum_{n=1}^{M} \Delta(n)}{M}$$

Şekil 2'de verilen örnek özelinde f_2, f_4 ve f_M frekanslarındaki sinyal güçleri (P_2, P_4 ve P_M) eşik sinyal güç seviyesinden (P_θ) daha güçlü oldukları için spektrum doluluk oranı hesaplamalarında dikkate alınırlar.

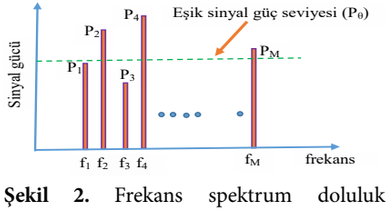

Şekil 2. Frekans spektrum doluluk hesaplama senaryosu

BULGULAR VE TARTIŞMA

RF Explorer 6G Combo spektrum analizörü kullanılarak ölçümü yapılan 50 MHz–2700 MHz arasına ait bir spektrum örneği Şekil 3'de verilmiştir. Şekilden de görüldüğü gibi ölçüm yapılan frekans spektrumunda baz istasyonu kaynaklı sinyal seviyeleri baskındır. FM (88 MHz–106 MHz) ve TV (174 MHz–230 MHz VHF bandı, 470 MHz–790 MHz UHF bandı) frekansların sinyal güçleri -60 dBm'den daha düşüktür (Tüm ölçüm sonuçları incelendiğinde FM ve TV frekanslarındaki sinyal gücü -60 dBm'den daha düşük olduğu için bu bantlar spektrum doluluk oranı değerlendirmelerine dahil edilmemiştir). En yüksek sinyal gücü -41,36 dBm ile 2137 MHz frekansında (UMTS2100 bandında) ölçülmüştür. Bu ölçüm için diğer en güçlü sinyal seviyeleri -43,93 dBm (942 MHz), -44,07 dBm (803 MHz) ve -50,01 dBm (1807 MHz) dir. 2G, 3G ve 4G teknolojilerini kullanan baz istasyonları için servis adları ve frekans bantları Tablo 2'de verilmiştir. Tablo 2'de verilen her bir servis için alt ve üst frekans değerleri Bilgi Teknolojileri ve İletişim Kurumu (BTK) tarafından tahsis edilmiş değerlerdir.

Tablo 2. Baz istasyonu servis adları ve kullanılan frekans aralıkları

Servis Adı	Alt frekans (MHz)	Üst frekans (MHz)
LTE800	791	820,9
LTE900	925,1	935,1
GSM900	935,1	961,0
GSM1800	1805	1820
LTE1800	1820	1879
UMTS2100	2010	2170
LTE2600	2570	2670

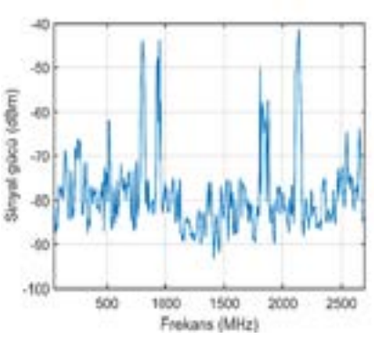

Şekil 3. 50 MHz – 2700 MHz arasına ait bir spektrum örneği

Sabit bir konumda, 4 saat aralıklarla kaydedilen 13 spektrum ölçümüne ait veriler (1) ve (2) eşitliğinde verildiği gibi analiz edilmiş ve spektrum doluluk oranları hesaplanmıştır. Hesaplanan SDO'nun yüzdelik değerlendirilmesi Şekil 4'de verilmiştir. Değerlendirmeler yedi farklı baz istasyonu servisi özelinde yapılmıştır. Değerlendirmelerde -50 dBm, -60 dBm ve -70 dBm eşik seviyeleri kullanılmıştır. Şekil 4'de eşik seviyesi bağlı olarak spektrum doluluk oranlarının değiştiği, büyük eşik değerleri için (örn. -50 dBm) spektrum doluluk oranının azaldığı görülmektedir. Ölçümlerde en yüksek doluluk oranı LTE900 servisi için hesaplanmıştır (-70 dBm eşik seviyesi için 12 ölçüm zamanında spektrumun tamamı doludur). En düşük doluluk oranı ise LTE2600 servisi içindir (-50 dBm ve -60 dBm için spektrum tamamen boştur). LTE2600 servisi için spektrumun bu denli boş olmasının temel nedeni olarak; ölçüm zamanında 4G'li baz istasyonlarının yeni kurulmaya başlanmış olması gerek sayılarının gerekse çıkış güçlerinin

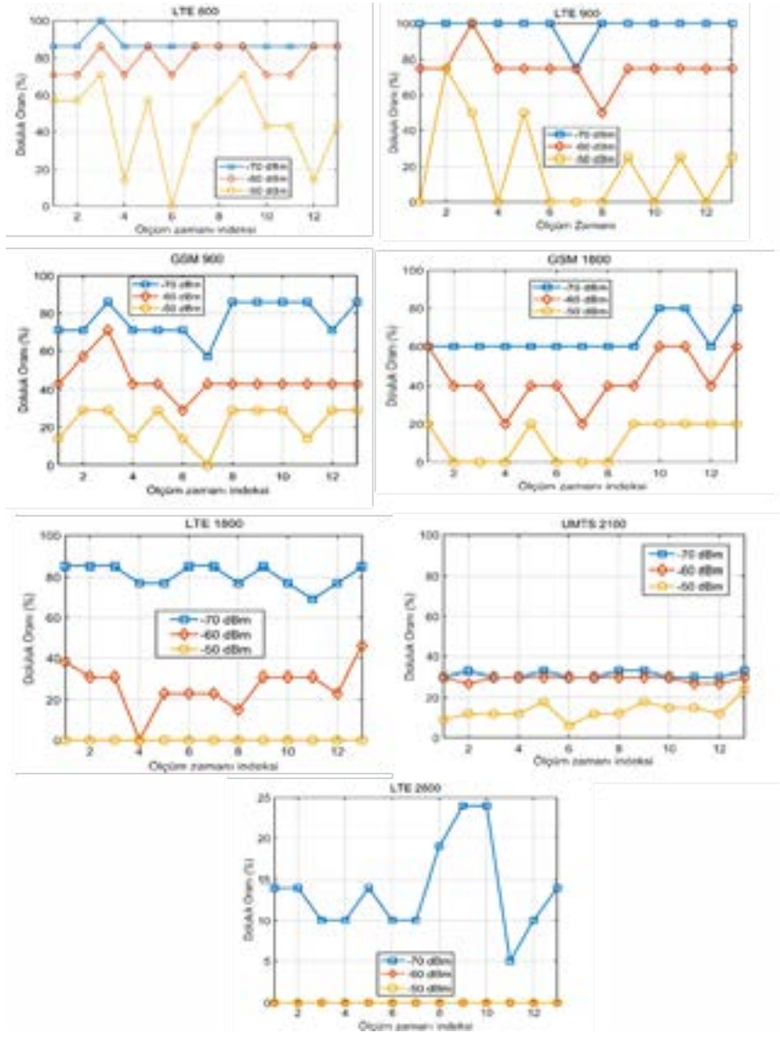

Şekil 4. Yedi farklı servis için ölçüm zaman indeksine bağlı spektrum doluluk oranları

az olması gösterilebilir. Şekil 4'den aynı servis ve aynı eşik seviyesi için dahi spektrum doluluk oranının ölçüm zamanına bağlı olarak değişkenlik gösterdiği görülmektedir. Bu değişkenlik %70'lere varan oranda olabilmektedir (örn. LTE800, -50 dBm için).

SONUÇLAR

Bu çalışmada, Ondokuz Mayıs Üniversitesi Kurupelit Yerleşkesinde 50 MHz – 2700 MHz frekans aralığında spektrumun en yoğun olduğu bir bölgede 13 farklı zamanda spektrum ölçümleri yapılarak, spektrum doluluk oranları incelenmiştir. Ölçümler 4 saat aralıklarla ve ardışık iki gün boyunca RF Explorer 6G Combo spektrum analizör kullanılarak yapılmıştır. Ölçüm konumunda baz istasyonu kaynaklı sinyal sevilerinin FM ve TV servislerine oranla çok daha yüksek olduğu görülmüştür. Baz istasyonu servislerinin gün içindeki genlik değişimleri -50 dBm, -60 dBm ve -70 dBm sinyal seviyeleri referans alınarak değerlendirmeler yapılmıştır. Ölçümlerden seçilen eşik seviyesine, seçilen baz istasyonu servisine ve ölçüm zamanına bağlı olarak spektrum doluluk oranlarının değiştiği görülmüştür. Bu değişim oranı -70 dBm eşik seviyesi için daha az iken -50 dBm eşik seviyesi için oldukça fazladır. Ölçümlerde en yüksek spektrum yoğunluğu %100 ile LTE900 (-70 dBm için) için, en düşük spektrum yoğunluğu ise %0 ile LTE2600 (-50/-60 dBm için) hesaplanmıştır. Ölçüm sonuçları bütün olarak değerlendirildiğinde ölçüm yapılan konumda baz istasyonu servisleri için tahsis edilen frekans bantlarının bilişsel radyo uygulamaları için kullanılabilir olduğu görülmüştür.

KAYNAKLAR

1. J. Mitola, G. Q. Maguire, "Cognitive radio: Making software radios more personal," IEEE Personal Communications, c. 6, s. 4, ss. 3–18, 1999.
2. S. Haykin, "Cognitive radio: brain-empowered wireless communications," IEEE Journal on Selected Areas in Communications, c. 23, s. 2, ss. 201–220, 2005.
3. Ç. Kurnaz, Z. E. Albayrak, "Measuring and evaluating TV white spaces in Samsun, Turkey," Journal of New Results in Science, c. 12, ss. 139–148, 2016.
4. Ç. Kurnaz, B. K. Engiz, Z. E. Albayrak, "Determination of TV white space spectrum availability in Samsun Turkey," 24th Telecommunications Forum (TELFOR), Belgrade, Serbia. 2016.
5. Z. E. Albayrak, Ç. Kurnaz, S. Karagöl, "Bilişsel Radyo Uygulamaları için Uzun Süreli Spektrum Doluluk Ölçümleri: Samsun Şehir Merkezi Örneği," Düzce Üniversitesi Bilim ve Teknoloji Dergisi, c. 8, s. 3, ss. 1840-1851, 2020.
6. B.K. Engiz, R. A. Rajab, "Spectrum Occupancy Measurements in Cellular Frequency Band in Samsun," Balkan Journal of Electrical & Computer Engineering, c. 9, s. 3, ss. 138–143, 2021.
7. H. Maloku, Z. L. Fazliu, M. Ibrani, A. Mekuli, E. Sela and M. Rajarajan. "Measurement of Frequency Occupancy Levels in TV Bands in Urban Environment in Kosovo," 18th Mediterranean Microwave Symposium (MMS), 31 October - 2 November, Prishtina, Kosovo, 2018.
8. E. Wiles, K. Negus. "Long-term Spectrum Monitoring and Occupancy from 174 to 1000 MHz in Rural Western Montana," 12th EuropeanConference on Antennas and Propagation (EuCAP 2018), 9-13 April, Butte, USA, 2018.
9. I. Şeflek, E. Yaldız. "Spectrum occupancy measurements at University Campus in Turkey," International Journal of Electronics and ElectricalEngineering, c. 5, s. 1, ss.1–6, 2017.
10. S. D. Barnes, P. A. Jansen van Vuuren and B. T. Maharaj. "Spectrumoccupancy investigation: Measurements in South Africa," Measurement, c. 46, s. 9, ss. 3098 – 3112, 2013.
11. J. Xue, Z. Feng and P. Zhang. "Spectrum occupancy measurements and analysis in Beijing," IERI Procedia, c. 4, ss.295–302, 2013.
12. B. K. Engiz, Y. A. Rajab. "Investigation of Spectrum Occupancy in GSM Band in Samsun, Turkey," 6th International Conference on Electrical and Electronics Engineering (ICEEE), Istanbul, Turkey, 2019.
13. Z. Qin, X. Zhou, L. Zhang, Y. Gao, Y. Liang and G. Y. Li, "20 Years of Evolution From Cognitive to Intelligent Communications," IEEE Transactions on Cognitive Communications and Networking, c. 6, s. 1, ss. 6–20, 2020.
14. Y. Arjoune, N. Kaabouch, "A Comprehensive Survey on Spectrum Sensing in Cognitive Radio Networks: Recent Advances, New Challenges, and Future Research Directions," Sensors (Basel), c. 19, s.126, ss. 1–32, 2019.
15. Z. Gu, T. Shen, Y. Wang and F. C. M. Lau, "Efficient Rendezvous for Heterogeneous Interference inCognitive Radio Networks," IEEE Transactions on Wireless Communications, c. 19, s. 1, ss. 91–105, 2020.
16. W. Zhang, Y. Sun, L. Deng, C. K. Yeo and L. Yang, "Dynamic Spectrum Allocation for Heterogeneous Cognitive Radio Networks With Multiple Channels," IEEE Systems Journal, c.13, s. 1, ss. 53–64, 2019.
17. RF Explorer, http://j3.rf-explorer.com/130, [Son erişim tarihi 26 Temmuz 2021].

OMÜ Mühendislik Bilimleri ve Teknolojisi Dergisi
OMU Journal of Engineering Sciences and Technology

e-ISSN: 2791-8858 OMU**JEST** September 2021, 1(1): 33-41

Çok Katmanlı Piezoelektrik Seramiklerin Dielektrik Özelliklerinin Sıcaklığa Bağlı Değişimlerinin İncelenmesi

Investigation of The Temperature Dependent Changes of The Dielectric Properties of Multilayer Piezoelectric Ceramics

Mert GÜL[1,*], Ayşe Gül TOKTAŞ[2,*], Hakan GÜLEÇ[3,*], Aydın DOĞAN[4,*]

[*] Nanotech İleri Tek. Malz. Elk-Elkt. Sis. San. Tic. A.Ş., Eskişehir, Türkiye

[1] Malzeme Bil. Ve Müh. Bölümü, Mühendislik Fakültesi, Afyon Kocatepe Üniversitesi, Afyonkarahisar, Türkiye
• **mertggg@gmail.com** • ORCİD > 0000-0001-8618-6261

[2] Malzeme Bil. Ve Müh. Bölümü, Mühendislik Fakültesi, Eskişehir Teknik Üniversitesi, Eskişehir, Türkiye
• **agakyurekli@gmail.com** • ORCİD > 0000-0002-5052-2574

[3] Nanotech İleri Tek. Malz. Elk-Elkt. Sis. San. Tic. A.Ş., Eskişehir, Türkiye
• **hkn.gulecc@gmail.com** • ORCİD > 0000-0002-1754-7470

[4] Malzeme Bil. Ve Müh. Bölümü, Mühendislik Fakültesi, Eskişehir Teknik Üniversitesi, Eskişehir, Türkiye
• **adogan@eskisehir.edu.tr** • ORCİD > 0000-0002-8122-2996

Makale Bilgisi / Article Information

Makale Türü / Article Types: Araştırma Makalesi / Research Article
Geliş Tarihi / Received: 28 Haziran / June 2021
Kabul Tarihi / Accepted: 18 Ağustos / August 2021
Yıl / Year: 2021 **| Cilt – Volume:** 1 **| Sayı – Issue:** 1 **| Sayfa / Pages:** 33-41

Atıf/Cite as: Gül, M., Toktaş, A. G., Güleç, H. ve Doğan, A. "Çok Katmanlı Piezoelektrik Seramiklerin Dielektrik Özelliklerinin Sıcaklığa Bağlı Değişimlerinin İncelenmesi - Investigation of The Temperature Dependent Changes of The Dielectric Properties of Multilayer Piezoelectric Ceramics". Ondokuz Mayıs Üniversitesi Mühendislik Bilimleri ve Teknolojisi Dergisi - Ondokuz Mayis University Journal of Engineering Sciences And Technology, 1(1), September :33-41

Sorumlu Yazar: Mert GÜL

ÇOK KATMANLI PİEZOELEKTRİK SERAMİKLERİN DİELEKTRİK ÖZELLİKLERİNİN SICAKLIĞA BAĞLI DEĞİŞİMLERİNİN İNCELENMESİ

ÖZ:

Çok katmanlı piezoelektrik seramiklerin üretimleri, katmanlar arasında değerli metal içeren iletken bir yapı kullanılarak yapılmaktadır. Bu iletken yapılar platin, paladyum, gümüş, altın içerikli olabilmektedir. Yaygın olarak kullanılanlardan bir tanesi de gümüş/paladyum (Ag/Pd) dur. Değerli metallerin oranı ise maliyetten dolayı düşürülmek istenmektedir. Bu çalışmada katkılı ve katkısız PZT-5A kompozisyonu kullanılarak 9/1, 7/3 ve 10/0 Ag/Pd içeriğine sahip çok katmanlı piezoelektrik seramikler üretilmiştir. Bu malzemelerin elektriksel özellikleri piezoelektrik seramiğin içeriğine ve sinterleme sıcaklığına bağlı olarak değişmektedir. Bu çalışmada piezoelektrik PZT-5A kompozisyonun içeriğine Li_2CO_3 katkılanarak sinterleme sıcaklığı düşürülmüştür ve böylece farklı paladyum oranına sahip Ag/Pd elektrot kullanılarak çok katmanlı seramik üretimi yapılabilmiştir. Farklı içerikteki iç elektrot kullanılarak üretilen seramiklerin uygulama sıcaklığına bağlı değişimleri de farklılık göstermektedir. Bu çalışmada 9/1, 7/3 ve 10/0 Ag/Pd elektrot kullanılarak üretilen çok katmanlı piezoelektrik seramiklerin 10˚C-100˚C arasındaki sıcaklık değişimine bağlı olarak piezoelektrik ve dielektrik özellikleri incelenmiştir. Yapılan çalışmadan elde edilen sonuçlara göre 10/0 Ag/Pd kullanılarak üretilen çok katmanlı piezoelektrik seramiklerin sıcaklığa bağlı dielektrik özellikleri diğer içerikteki elektrot malzemeler kullanılarak üretilen çok katmanlı seramiklerden daha fazla değişime uğramıştır.

Anahtar Kelimeler: *Çok katmanlı; Piezoelektrik; Sıcaklık; Dielektrik; PZT*

INVESTIGATION OF THE TEMPERATURE DEPENDENT CHANGES OF THE DIELECTRIC PROPERTIES OF MULTILAYER PIEZOELECTRIC CERAMICS

ABSTRACT:

The production of multilayer piezoelectric ceramics is made using a conductive structure containing precious metals between layers. These conductive structures can contain platinum, palladium, silver and gold. One of the commonly used ones is silver/palladium (Ag/Pd). The ratio of precious metals is desired to be reduced due to cost. In this study, multilayer piezoelectric ceramics with 9/1, 7/3 and 10/0 Ag/Pd contents were produced using doped and undoped PZT-5A composition. The electrical properties of these materials vary depending on the content of the piezoelectric ceramic and the sintering temperature. In this study, the sintering temperature was reduced by adding Li_2CO_3 to the piezoelectric PZT-5A composition and thus multilayer ceramic prodution could be made by using Ag/Pd electrode with different palladium ratio. Variations of ceramics produced using inner electrodes with different contetns also differ depending on the application temperature. In this study, piezoelectric and dielectric properties of multilayer piezoelectric ceramics produced with 9/1, 7/3 and 10/0 Ag/Pd were investigated depending on the temperature change between 10˚C-100˚C. According to the results obtained from the study, the temperature dependent dielectric properties of the multilayer piezoelectric ceramics produced with 10/0 Ag/Pd electrode have changed more than the multilayer ceramics produced using other electrode material.

Keywords: *Multilayer; Piezoelectric; Temperature; Dielectric; PZT*

Öne çıkanlar

Çok katmanlı piezoelektrik seramikler yüksek hassasiyet ve yüksek mekanik mukavemet isteyen uygulamalarda kullanılabilmektedir. Bu çalışmada çok katmanlı piezoelektrik seramikler düşük sıcaklıkta sinterlenebilen katkılı PZT-5A kompozisyonlar ve farklı Ag/Pd içeriğine sahip elektrotlar kullanılıp şerit döküm yöntemiyle üretilerek sıcaklığa bağlı değişimleri incelenmiştir. Burada Ag/Pd oranı iletken özellik kazanması için gerekli olan sinterleme sıcaklığını değiştirmektedir. Bu sebeple eniyileştirme yapılarak farklı sıcaklıkta yapılan uygulamalar için çalışma gerçekleştirilmiştir

GİRİŞ

Piezoelektrik malzemeler havacılık, uydu ve uzay teknolojileri, savunma sanayi, otomotiv ve biyomedikal uygulamalar, imalat sanayi ve elektrik-elektronik sektörü gibi birçok sektörde sensör ve aktüatör olarak kullanım alanına sahiptir. Piezoelektrik seramikler, ultrasonik görüntüleme, su altı görüntüleme, dizel injeksiyon sistemleri ve hassas deplasman kontrol uygulamaları gibi uygulamalarda kullanılmaktadır. Bu uygulamalardaki ihtiyaçlara yönelik olarak yüksek mekanik dayanıma ve düşük sürüm voltajına sahip piezoelektrik seramiklere gereksinim duyulmuştur. Çok katmanlı seramikler bu ihtiyaçtan doğmuştur [1]. 10-300 mikron kalınlığında seramik-polimerik katmanlar şerit döküm yöntemiyle üretildikten sonra elektrotlanarak üstüste getirilir. Bu katmanlı yapı sinterlenip terminasyonu yapıldıktan sonra polarize edilir ve çok katmanlı seramikler böylece üretilmiş olur. Bu seramiklerin üretimleri, katmanlar arasında değerli metal içeren iletken bir yapı kullanılarak yapılmaktadır. Bu iletken yapılar platin, paladyum, gümüş, altın içerikli olabilmektedir. Ag/Pd karışımı ise maliyet düşürme çalışmaları kapsamında çok katmanlı seramiklerin üretiminde kullanılmaktadır [2].

Aktüatör uygulamalarında kullanılan piezoelektrik malzemelerin farklı sıcaklık uygulamalarına bağlı olarak elektriksel özelliklerinde düşüş meydana gelmektedir. Kurşun içerikli PZT tabanlı malzemelerin sıcaklığa bağlı elektriksel özelliklerinin davranışları uzun yıllardır araştırılmaktadır. Aktüatör uygulamalarında sıcaklığa bağlı elektriksel özelliklerin değişimi davranışı tahmin edilebilir malzemeler geliştirilerek ürün kayıpları belirlenebilir.

Farklı fazlardaki kompozisyonlara ve Morfotropik Faz sınırı kompozisyonlarındaki sıcaklık değişiminin elektriksel özelliklere etkisini görmek üzere PZT ince filmler üzerinde yapılan çalışmada dielektrik sabite ve d_{33} değerinin arttığının ancak 30/70 oranında Zr/Ti içeren kompozsiyonun değerinin diğer kompozisyonlara nazaran daha az olduğu görülmüştür. Bu durum Curie sıcaklığının daha yüksek olmasıyla açıklanmıştır [3]. Nb-Li içeren PZT kompozisyonunda dielektrik sabite değeri oda sıcaklığında 1800 değerinden 250˚C'de 4000 değerine, d_{33} değeri ise 330 pC/N değerinden 680 pC/N değerine ulaşmıştır [4]. PZT-5H kompozsiyonunda 0-40˚C arasındaki dielektrik sabite değişiminin %33 değerine ulaşabileceği [5] belirtilmiştir. PZT tabanlı PZT-4, PZT-5A ve PZT-5H tip piezoelektrik seramiklerde yapılan çalışmalarda dielektrik sabitesi değeri PZT-5H seramiklerde düşük sıcaklıklarda daha fazladır. Koersif elektrik alan değerleri düşmüş olup, PZT-5H tip seramiklerde düşüşün daha fazla olduğu görülmektedir [6]. Bunun yanında çok katmanlı seramiklerin de sıcaklığa bağlı eletriksel özellikleri değişimlerine yönelik çalışmalar mevcuttur [7]. Ancak hem kompozisyonel içeriği farklı hem de iç elektrot pişirim sıcaklığı farklı olarak üretilen yekpare (bulk) seramik ve çok katmanlı seramiklerde bu değişim incelenmemiştir. Bu çalışmada ise sıcaklık farklılığının iç elektrottan mı yoksa kompozisyondan mı kaynaklandığını görmek üzere hem kompozisyondan üretilen peletlerde sıcaklık çalışması yapılmış hem de farklı iç elektrot kullanılarak üretilen çok katmanlı seramiklerin sıcaklığa bağlı davranışları incelenmiştir. Bu sayede farklılığın kompozisyonel özelliklerden, iç elektrot malzemesinden veya bu ikisinin etkileşiminden kaynaklanma oranı gözlenebilecektir.

MATERYAL VE YÖNTEMLER

Bu çalışmada ticari olarak kullanılan PZT-5A tozuna 0.1wt% ve 0.2 wt% oranlarında Li_2CO_3 katkılanmıştır. Elde edilen kompozisyonlar 24 saat boyunca etanol ortamında bilyalı değirmende zirkon bilyalarla karıştırma-öğütme işlemine tabi tutulmuşlardır. Elde edilen kompozisyon karışımları döner kurutucuda kurutulmuş ve preslenebilmesi için PVA bağlayıcı eklenmiştir. Bağlayıcısı eklenen toz kompozisyonları ve PZT-5A tozu 1.5 ton/cm^2 oranında ön şekillendirilmiş ve sonrasında 200 MPa eşeksenli olarak preslenmişlerdir. Bu presleme sonrasında elde edilen pelet numuneler; PZT-5A için 1250˚C-2saat, 0.1wt% Li_2CO_3 katkılanmış numuneler 975˚C-4 saat ve 0.2wt% Li_2CO_3 katkılanmış numuneler ise 875˚C-4saat alumina pota içerisinde sinterlenmişlerdir. Sinterlenme sonucunda elde edilen peletler yüzey paralelliği sağlandıktan sonra iletken özellik sağlanması için elektrotlanmışlardır. Elektrotlanan numuneler 2.4 kV/mm değerinde 90-100 ˚C sıcaklıktaki yağ banyosu içerisinde polarize edildikten sonra elektriksel ölçümleri Agilent 4294A kazanç-faz analizöründe yapılmıştır. d_{33} değerleri ise Sinocera YE2370 d_{33}metre kullanılarak yapılmıştır.

Çok Katmanlı Seramik Üretimi

Plastikleştirici, bağlayıcı ve köpük giderici olarak adlandırılan polimerik malzemeler ve kompozisyon üretimi sonucu elde edilen PZT toz karışımları şerit döküm çamuru hazırlamak üzere 24 saat boyunca bilyalı sistemde karıştırılmışlardır. Şerit döküm cihazı kullanılarak 55-65 mikron kalınlığında dökülüp kurutularak elde şeritler daha sonra 7/3 Ag/Pd (Gümüş paladyum), 9/1 ve 10/0 elektrot pasta ile elektrotlanmışlardır. Elektrotlanan şeritler 50 Bar basınçla üstüste getirilmiş, 60°C sıcaklık altında yapışmaları sağlanmıştır. Elde edilen katmanlanmış yığınlar elektrot desenine uygun şekilde kesilmişlerdir. Kesilen ham malzemeler 50˚C sıcaklık altında 15 MPa basınçla birlikte 3 dk boyunca yoğunlaştırılmışlardır. Yoğun haldeki farklı Ag/Pd oranındaki elektrotlara sahip ham seramikler 875˚C-1120˚C aralığındaki farklı sıcaklıklarda 4 saat boyunca sinterlenmişlerdir. Çok katmanlı seramik üretim akım şeması şekil 1'de verilmiştir.

Şekil 1. Çok katmanlı seramik üretim akım şeması [8]

Çok katmanlı seramik üretiminde kullanılan metal tabanlı iç elektrot ve seramiklerin ısıl genleşme katsayıları farklıdır. Bu farklılık sinterleme esnasında malzemelerde laminasyon problemlerine, çatlaklara ve kırılmalara sebep olmaktadır. Bu hatalar çok katmanlı seramiklerde güvenlik problemlerini ortaya çıkarmaktadır.

Sinterleme sonrasında elde edilen seramiklerin önce yüzey işlemleri yapıldıktan sonra dış terminasyon elektrotları yapılmıştır. Elektriksel bağlantıları yapılan seramikler 60°C'de 5 dakika süresince polarize edilmişlerdir. Agilent 4294 A Kazanç-Faz analizöründe elektriksel ölçümleri yapılmıştır. Şekil 2'de, sinterlenerek yüzey işlemleri yapılan çok katmanlı seramik ve şematik görünümü verilmiştir.

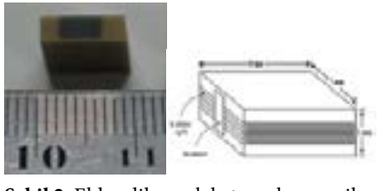

Şekil 2. Elde edilen çok katmanlı seramik ve şematik görünümü

Sıcaklık Testleri

Sıcaklık testleri için Polyscience yağ banyosu içerisine tüp daldırılarak sıcaklık değişimleri oluşturulmuştur. Bu tüp içerisine ayrıca termokupl daldırılarak sıcaklık ölçümleri yapılmıştır. Bu esnada sıcaklık istenilen değerlere ulaşınca Agilent 4294 A cihazında 1 kHz değerinde kapasintans ölçümleri

yapılmıştır. Dielektrik sabite değeri şu şekilde hesaplanmaktadır.

$$K^T = \frac{tC}{A\varepsilon_0} \quad (1)$$

Burada t (m) numunenin kalınlığı, C (nF) kapasitansı, A (m^2) yüzey alanı, ε_0 ise havanın dielektrik sabitesi ($8{,}85x10^{-12}$ F/m) alan ve kalınlık değeri aynı olan numunelerde belirleyici özellik olarak sunulmuştur.

BULGULAR VE TARTIŞMA

Lityum atomunun atom boyutu yaklaşık olarak (0,74˚) olarak verilmektedir. Literatürde yer alan bilgilere göre ABO_3 perovskit yapısında B yerleşimine atom boyutu yakın olan Ti^{4+} atomunun (0,61A˚) yerine yerleşerek, latis boyunun uzamasına ve tetragonalliğin artmasına neden olmaktadır. X-ışını deseni sonuçları bu bulguyu desteklemektedir [9]. Li_2CO_3 katkısıyla birlikte mikroyapıda da belirgin değişmeler bulunduğu kayıtlara geçmiştir [10]. Yapılan çalışmada katkısız ve katkılı seramiklerin mikroyapısında değişimler elektron mikroskobu aracılığıyla incelenmiştir (Şekil 3).

Mikroyapı görüntüleri incelendiğinde Li_2CO_3 katkısıyla birlikte sıvı faz kalıntılarının tane aralarında oluştuğu görülmektedir. Ayrıca literatürle de uyumlu olarak Li_2CO_3 katkısı yapıldığında tane boyutunun düştüğü görülmektedir. Bunun yanında Li_2CO_3 katkısıyla birlikte yapıda yer yer boşlukların oluştuğu gözlenmektedir. Bunun nedeninin ise Li_2CO_3 uçuculuğu olduğu söylenmektedir [11].

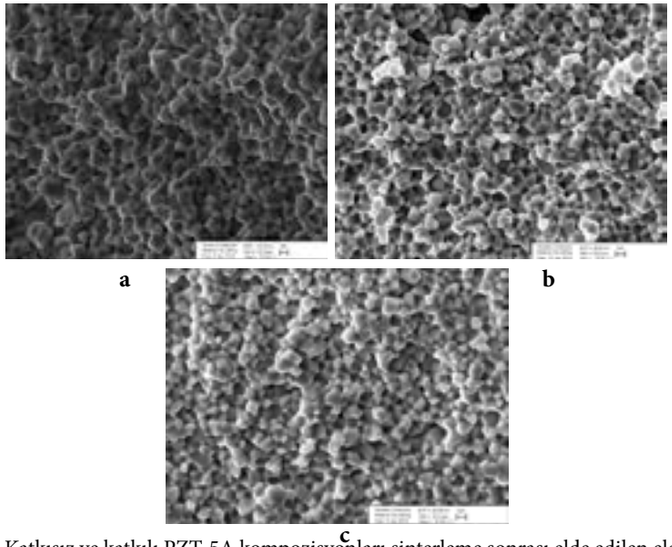

Şekil 3. Katkısız ve katkılı PZT-5A kompozisyonları sinterleme sonrası elde edilen elektron mikroskobu görüntüleri a) katkısız PZT-5A seramik b) 0.1% Li_2CO_3 katkılı yekpare PZT-5A seramik c) 0.2% Li_2CO_3 katkılı yekpare PZT-5A seramik.

Tablo 1. Lityum katkılı ve katkısız kompozisyonla üretilen yekpare pelet numunelerin elektriksel özellikleri

Li_2CO_3 katkısı%	Sıcaklık (°C)	d_{33} (pC/N)	Q_E	tan δ	k_t	Q_m	K^T
0.0	1250°C	600	58	0.0172	0.65	66	3881
0.1	975°C	580	53	0.0188	0.60	64	3435
0.2	875°C	710	42	0.0238	0.64	49	3990

Katkısız ve katkılı kompozisyonlar kullanılarak üretilen peletlerin piezoelektrik özellikleri Tablo 1'de verilmektedir.

Bu tabloya göre farklı Li_2CO_3 katkılarıyla ve farklı sıcaklıklarda sinterlenen pelet seramiklerin özellikleri nispeten çok büyük farklılık göstermemektedir. d_{33} değerleri 580 ile 710 pC/N aralığında değişmektedir. Kapling sabitesi olarak adlandırılan k_t değeri ise 0.6' dan büyüktür. Dielektrik sabitesi değeri olan K^T değeri 3500 ve üzerindedir. Kayıp faktörü olan tan δ değerleri birbirine yakındır. Mekanik kalite faktörü değeri olarak adlandırılan Q_m değeri, katkısız kompozisyon değerine nispeten yakındır. Bu sonuca bakılarak uygulama alanlarında birbirlerinin yerlerine kullanılabileceklerdir. Pelet numunelerin dielektrik sabite değerinin sıcaklığa bağlı değişimi karşılaştırmalı olarak Şekil 4'te verilmektedir.

Piezoelektrik malzemelerin özellikleri iki farklı mekanizmanın kombinasyonuyla açıklanır. Tek domainin hareketi içsel katkılar olarak adlandırılır. Malzemenin domain hareketi gibi diğer bileşenlerinin etkisine ise dışsal katkılar denmektedir. İçsel katkıların etkisi hacme uygulandığında çok küçük olmaktadır. Ancak dışsal katkıların etkinliği özellikle domain duvarı hareketliliği, atomların sahip olduğu enerji ile ilgili olduğundan sıcaklık arttıkça atomların enerjileri artar. Bu etkiyle birlikte domain duvarı hareketliliği de artar [12]. Sıcaklık etkisiyle birlikte dielektrik sabitesi artması dielektrik malzemelerde bilinen bir fenomendir [13]. Burada sıcaklığa bağlı olarak değişimin nasıl olduğu ve yüzde değeri takip edilmektedir. Lityum katkısı arttıkça malzemenin tane aralarındaki boşlukların arasına sıvı faz yerleşmekte ve bunun sonucunda dielektrik sabite değeri artmaktadır. Li_2CO_3 katkısıyla sıcaklığa bağlı olarak değişim artmaktadır. Katkısız PZT-5A kompozisyonunda değişim %58 iken, %0.1 Li_2CO_3 katkı yapıldığında %63 değerine %0.2 Li_2CO_3 katkı yapıldığında ise %67 değerine ulaşmaktadır.

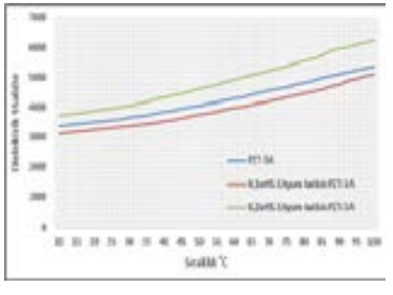

Şekil 4. Farklı Li_2CO_3 katkılı pelet numunelerin dielektrik sabite değerlerinin sıcaklığa bağlı değişimi

Çalışmanın devamında katkılı ve katkısız PZT-5A kompozisyonu kullanılarak üretilen farklı iç elektrotlara sahip çok katmanlı seramiklerin sıcaklığa bağlı olarak değişimi incelenmiştir.

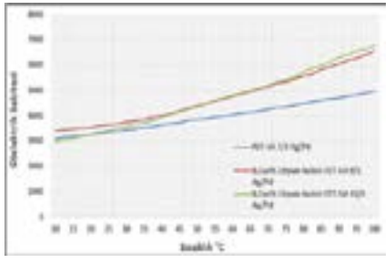

Şekil 5. Farklı iç elektrot kullanılarak üretilen çok katmanlı seramiklerin dielektrik sabite değerlerinin sıcaklığa bağlı değişimi

Katkısız PZT-5A ve 7/3 Ag/Pd kullanarak üretilen çok katmanlı seramiklerde değişim %48 iken, %0.1 Li_2CO_3 katkı yapıldığında ve %91 değerine %0.2 Li_2CO_3 katkı yapıldığında ise %128 değerine ulaşmaktadır. Değişim oranları tablo halinde verilmektedir (Tablo 2).

Tablodan görüldüğü üzere sıcaklık değişimine bağlı olarak çok katmanlı seramiklerde katkısız yekpare seramik kompozisyonunun, katkılı kompozisyonlara göre sıcaklık değişimi daha azdır. Ancak sıcaklığa bağlı bu yüzdelik değişim lityum katkısı artırıldığında çok fazla artmaktadır. Piezoelektrik malzemelerin dielektrik sabite değerlerinin sıcaklığa bağlı olarak değiştiği bilinmektedir. Li_2CO_3 katkısıyla birlikte sıcaklık değişimi yaklaşık olarak 10% oranında artmaktadır. İç elektrottan kaynaklandığı düşünülen sıcaklık değişimi oranı ise yaklaşık olarak 30%'dur. Bu farklılığın iletken elektrot pastanın içeriğideki gümüş ve paladyumun ısıl iletkenlik farklılıklarından kaynaklanabileceği düşünülmektedir. Sıcaklığa bağlı yüzde değişimlerin bir kısmı kompozisyonel etkilerden kaynaklanmakta, bir kısmı ise hem metal-seramik arayüzündeki etkileşimden hem de iç elektrotun içeriğinden kaynaklanmaktadır.

Tablo 2. Farklı özelliklerdeki yekpare ve çok katmanlı seramiklerin sıcaklığa bağlı Dielektrik Sabite değişimi

Özellikler		% Değişim	
Katkı oranı	**Kullanılan elektrot**	**Yekpare**	**Çok Katmanlı Seramik**
Katkısız	7/3 Ag/Pd	58	48
%0.1 Li2CO3 katkılı	9/1 Ag/Pd	63	91
%0.2 Li2CO3 katkılı	10/0 Ag/Pd	67	128

SONUÇLAR

Bu çalışmada farklı Ag/Pd oranındaki iç elektrotlara sahip PZT-5A kompozisyonu kullanılarak üretilen çok katmanlı piezoelektrik seramiklerin sıcaklığa bağlı dielektrik özellikleri ölçülmüştür. Bu kapsamda farklı Ag/Pd içerik oranına ve bu sebeple farklı sinterleme sıcaklığına sahip çok katmanlı piezoseramik üretimi için daha düşük sinterleme sıcaklığına sahip PZT-5A kompozisyonu geliştirilmiştir. Farklı Ag/Pd içeriğindeki elektrot pastaların etkilerini gözlemlemek üzere piezoelektrik seramik pelet numuneler üretilmiş ve bunların sıcaklığa bağlı dielektrik özellikleri de incelenmiştir. Bu çalışmada çıkan sonuçlara göre sinterleme sıcaklığını düşüren Li_2CO_3 katkısı dielektrik sabite değişiminde %10 luk bir değişime yol açmaktadır. 10/0 Ag/Pd iç elektrot pasta ise %60 oranında dielektrik sabite değişimine sebebiyet vermektedir. Bu oranlardaki malzemeler kullanılacaksa kompozisyonel içeriğin sıcaklığa bağlı değişimlerinin de incelenmesi gerekmektedir. Özellikle dizel enjeksiyon sistemlerinde ve hassas deplasman kontrolü gereken sistemlerde çok katmanlı seramiklerin ve sistem tasarımlarının sıcaklık farklılıklarına uygun şekilde yapılması gerekmektedir. Uygulamalarda bu etki gözönünde bulundurulmalıdır.

Teşekkür

Deneysel çalışmalardaki yardımlarından ötürü Nebahat Bıyıklı'ya, Ali Bıyıklı ve Görkem Hatipoğlu'na teşekkürler.

KAYNAKLAR

1. Uchino K., Takahashi S., "Multilayer Ceramic Actuators, Current Opinion, Ceramics," Composites and Intergrowths, ss. 698- 705, 1996.
2. I.H. Im, H.S. Chung, D.S. Paik, C.Y. Park, J.J. Park, S.G. Bae "Multilayer piezoelectric actuator with AgPd internal electrode" Journal of the European Ceramic Society, c.20, ss. 1011-1015, 2000.
3. H. Maiwa, S.H. Kim, N. Ichinose "Temperature dependence of the electrical and electromechanical properties of lead zirconate titanate thin films" Applied Physics Letters c. 83, ss. 4396, 2003.
4. C. Miclea, C. Tanasoiu, L. Amarande, M. Cioangher, L. Trupina, C.T. Miclea, C.David "Temperature Dependence Of The Main Piezoelectric Parameters Of A Nb-Li Doped Pzt Ceramic" 2006 International Semiconductor Conference, ss. 279-282, 2006.
5. M. G. Cain. Characterisation of Ferroelectric Bulk Materials and Thin Films, London, UK, Springer, 2014.
6. M. W. Hooker "Properties of PZT-Based Piezoelectric Ceramics Between-150 and 250°C" NASA / CR- 1998-208708.
7. J. Pritchard, C. R. Bowen, F. Lowrie "Multilayer actuators: review" British Ceramic Transactions, c.100, ss. 265-274, 2001.
8. M. Gül. Çok katmanlı Piezoelektrik Seramiklerin Tasarımı, Üretimi ve Elektriksel Yorulma Davranışlarının Karakterizasyonu. PhD, Afyon Kocatepe Üniversitesi, Afyonkarahisar, Türkiye, 2019.
9. L.D. Vuong, P.D. Gio "Effect of Li2CO3 addition on the sintering behavior and physical properties of PZT-PZN-PMnN ceramics" International Journal of Materials Science and Applications, c.2, ss. 89-93, 2013.
10. Y.D. Hou, L.M. Chang, M.K. Zhu, X.M. Song, H. Yan "Effect of Li2CO3 addition on the dielectric and piezoelectric responses in the low-temperature sintered 0.5PZN–0.5PZT systems" Journal Of Applied Physics, c. 102, ss. 084507, 2007.
11. J. Yoo, C. Lee, Y. Jeong, K. Chung, D. Lee, D. Paik. "Microstructural and piezoelectric properties of low temperature sintering PMN-PZT ceramics with the amount of Li2CO3 addition." Materials Chemistry and Physics, c.90, ss.386–390, 2005.
12. S Davoudi. Effect of Temperature and Thermal Cycles on PZT Ceramic Performance in Fuel Injector Applications. MSc, University of Toronto, Canada, 2012.
13. A.J. Moulson, J.M. Herbert. Electroceramics, 2nd ed. West Sussex, İngiltere, John Wiley & Sons Ltd, 2003.

OMÜ Mühendislik Bilimleri ve Teknolojisi Dergisi
OMU Journal of Engineering Sciences and Technology

e-ISSN: 2791-8858 OMU**JEST** September 2021, 1(1): 43-57

Analysis of The Flood Flow Rate In Karpuz Basin in Antalya, Turkey

Tuğba ÖZKOCA[1], Aslı ÜLKE KESKİN[2]

[1] MSc., State Hydraulic Works, 13th Regional Directorate, Antalya, Turkey
• **tugbasafak@dsi.gov.tr** • ORCID > 0000-0002-9959-478X

[2] Department of Civil Engineering, Faculty of Engineering, Ondokuz Mayıs University, Samsun, Turkey
• **asli.ulke@omu.edu.tr** • ORCID > 0000-0002-9676-8377

Makale Bilgisi / Article Information

Makale Türü / Article Types: Araştırma Makalesi / Research Article
Geliş Tarihi / Received: 28 Haziran / June 2021
Kabul Tarihi / Accepted: 16 Eylül / September 2021
Yıl / Year: 2021 **| Cilt – Volume:** 1 **| Sayı – Issue:** 1 **| Sayfa / Pages:** 43-57

Atıf/Cite as: Özkoca, T. ve Ülke Keskin, A. "Analysis of The Flood Flow Rate In Karpuz Basin in Antalya, Turkey". Ondokuz Mayıs Üniversitesi Mühendislik Bilimleri ve Teknolojisi Dergisi - Ondokuz Mayis University Journal of Engineering Sciences And Technology, 1(1), September 2021: 43-57.

Sorumlu Yazar: Tuğba ÖZKOCA

ANALYSIS OF THE FLOOD FLOW RATE IN KARPUZ BASIN IN ANTALYA, TURKEY

ABSTRACT:

Flood disaster occurs when there is more water in the riverbed than its capacity, and results in loss of life and other damage. Therefore, the determination of flood flow rates is very important to reduce the effects that may occur after the flood. To prevent flood damages economically with engineering structures, it is necessary to examine floods and to determine the recurrence time and size. Flood flow calculations are a project process in which many parameters vary on each basin modeled, which causes very different results to occur even in a single parameter within many methods. Flow gauging station or improved empirical methods are used to calculate flood flow magnitude. There is more than one method in the flood calculation. Each method has different assumptions according to basin characteristics. In this study, analysis of the flood flow rate using DSI Synthetic, Mockus and Regional Frequency Analysis methods in Karpuz basin in Antalya. Netcad / NETHYDRO software module was used in the analysis and model design phases of the study. As a result of the comparisons, it was seen that the DSI Synthetic method, where the increment flows were calculated, gave greater flow values than the Mockus method and Regional Frequency.

Keywords: *Basin, DSI Synthetic, Mockus, Regional Frequency Analysis, Nethydro*

INTRODUCTION

The negative impact of the rapidly increasing world population on natural resources is rising day by day. Especially in developing countries, industrial studies and wrong land uses cause water resources, which are extremely important for human life, disappearing. This situation in the world emphasizes the importance of the management of water, which is a limited resource. Water resources should be managed following the principle of sustainable development because of the basin and other natural resources. The main target in basin management; the conservation of natural resources, a renewable environment of the environment and the sustainable management of resources. Therefore, the main target in watershed management; the conservation of natural resources, the transformation of the environment into a renewable environment and the sustainable management of resources [15]. Hydrological Modeling is a set of operations to make an unknown goal simple and understandable, based on available sources. Also, modeling studies allow us to see how many events are shaped or shaped under past, present and future conditions. Concurrently modeling is the process of applying the basic knowledge and experience to evaluate the simulation or an actual system performance to achieve specific goals. In the modeling stage, the model synthesis is integral components for the comparison of measurement and observation of the real system [8]. A hydrological model can be considered as similar to the hydrological system in nature. The concept of the system is of great importance in hydrological studies. The system is a set of components that are related to each other in a regular manner and which form a whole by separating a certain limit from their surroundings. The system is based around the dividing line to be drawn to the problem being examined [2]. Computer models have been used in hydrology in the mid-1960s with the Stanford Watershed Model. The software, which can simulate the amount and quality of rain flow, was prepared by the US Environmental Protection Agency (US-EPA) in the early 1970s [9]. A wide range of hydraulic and hydrological models has been developed over the years from simple to complex [19]. Process models based on streamflow are named as low flow models and rainfall - flow models. The amount of flow in a stream is determined by the periods in which precipitation flows. It is determined by using the withdrawal coefficients in dry periods where there is no precipitation in low current draw models [11].

Camarasa and Tilford, [3]., in their study, rainfall-flow transfer function was applied to seasonal flows in Spain. Flow simulations have been conducted for two small catchments (Carraixet and Poyo basins), located in near another yet with significantly different geological characteristics. It was observed that the basin, which was measured by this application, had good results when it was a basin that reacted quickly to precipitation. In a study by Jennings et al [7], in Ireland, they applied a water budget approach to seven test basins to quantify river flow elements with NAM (NedbØr- AfstrØmnings-Model) rainfall-runoff model, which is a module of DHIs MIKE 11 modeling suite. The results from these pilot catchments have been used to develop a decision model based on catchment descriptors from GIS datasets for the selection of NAM parameters. Tayfur and Singh [17] used artificial neural networks and fuzzy logic methods to estimate event-related precipitation-flow and tested these models according to the kinematic wave approach. In the fuzzy logic model, they used triangle membership functions for input and output variables. Three models were found to be suitable for experimental data and it was observed that this study yielded better results for estimation models applied for small basins, ANN and fuzzy logic models. In Turkey, Gürkan [6] has evaluated the effects of climate change in the Seyhan River Basin. The mathematical model created with the Mike-She basin model has been found to simulate superficial flow and storage, evaporation, transpiration, flow in the non-saturated area, groundwater feed and streamflow. The result of the study Seyhan Basin high sensitivity to climate change and precipitation and temperature change in both the basin surface water potential as well as groundwater feeding. In another study by Günal and Güven [5], synthetic unit hydrograph parameters are calculated by using Synder, Mockus, SCS (Soil Conservation Service) and DSI (State Hydraulic Works) methods at Damlıca, Vize, and Kumdere. They compared peak discharge and base time for all methods used. Şarlak and Tiğrek

[13], have calculated the flood flow magnitude of Kayraktepe Dam with the nonparametric approach based on K nearest neighbors (KNN). They detected although quantile estimates for 500 years return period was 2363.95 m^3/s in the past feasibility report, this value descended to 1814.83 m^3/s with the nonparametric approach. They also concluded that the study will contribute to the design flow of the dam. Çetiner [4] modeled the Ergene Basin according to the Taudem Algorithm and calculated the flood flow of the Ova Stream according to the DSİ Synthetic and Mockus methods. Netcad GIS software has benefited from the Nethydro module in all stages of its operation. According to the DSİ Synthetic and Mockus method, the flood flow rates calculated at different repetition intervals were compared.

In this study, flood analysis was performed by hydrological analyzes. According to the synthetic methods, Mockus and DSI Synthetic methods precipitation values of different frequencies were calculated by using precipitation values of meteorological precipitation stations, rate of impact on the basin, precipitation analyzes and flow curve number. Besides, in this study, Regional Frequency Analysis was used in flood flow calculations. Netcad/NETHYDRO software was used in the analysis and model design phases of the study. All methods have been applied and the most suitable flood flow for the modeled basin has been compared.

MATERIALS AND METHODS

Project Area

The location of the project is Karpuz Stream, which is the combination of Karpuz and Çingen streams in Kızılot and Taşkesiği areas within the boundaries of Manavgat District of Antalya Province (Figure 1). In the basin where Karpuz Stream is located, climatic differences are observed between the parts close to the coast and the mountains. The coastal areas are hot and dry in summer, summer and spring are quite rainy. While the precipitation rate is high in the coastal areas, the amount of rainfall decreases in the inner parts. However, since the snow load is high at the upper elevations, the flow rate is also high during the snow-melting season.

Figure 1. Project Area: Antalya Karpuz Stream

Methods

There is more than one method in the flood calculation. Each method has different assumptions according to basin characteristics. Therefore, accounts for the same basin can give different results. The determination of which method gives the most appropriate result is obtained by interpreting the account results together with the field surveys by the engineer. For this purpose, after the calculations are made in the office, the slope and size of the streambed in the project section are examined and the flow rate that the existing bed can spend is calculated approximately. The choice of method in flood calculation by synthetic methods is made according to the size of the basin to be calculated except Mc Math method [10]. However, the accuracy of this acceptance is not definite. Method applications according to the size of the basin are given in Table 1.

Table 1. Methods calculating flow rate

Methods	Application Area (A)(km^2)
Rational Method	A< 5 km^2
Mockus Method	5km^2 < A(km^2) <50 km^2
DSI Synthetic Method	10 km^2<A (km^2) <1000 km^2
Synder Method	A> 1000 km^2
Mc Math Method	flat areas

Modeling of Basin with Netcad – NetHydro

TauDEM (Terrain Analysis Using Digital Elevation Models) algorithm developed by Tarboton [16] was used to determine basin boundaries (Figure 2). This algorithm determines the basin boundaries because of various analyzes by using the digital terrain model as input data.

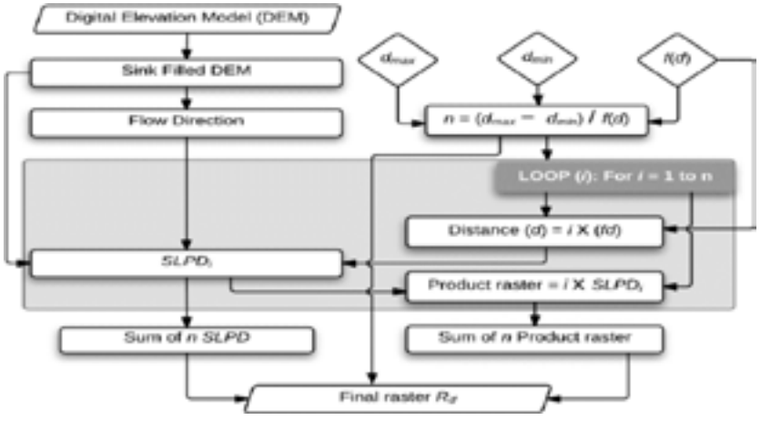

Figure 2. TauDEM Algorithm

Modeling of basins with digital terrain data

For the basins to be modeled, the raster data containing the TIN model or elevation information should be added to the project (Figure 3). Triangular models are created in Figure 4 in all basins with digital terrain data.

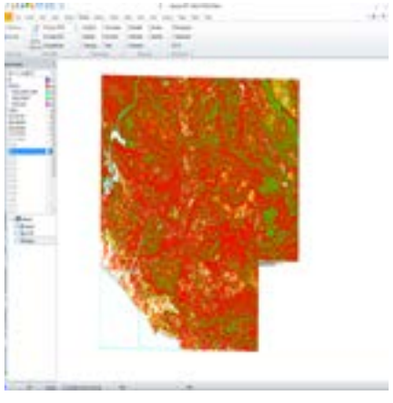

Figure 3. Digital Terrain Model of the Study Area

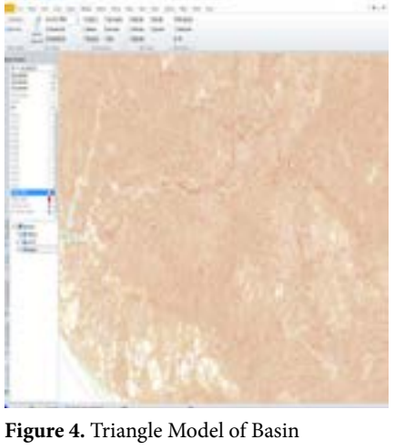

Figure 4. Triangle Model of Basin

Modeling of basin according to downstream point

First of all, the Antalya-Manavgat sub-basin is modeled as a major part of the basins where the surface waters of the basin where Karpuz Stream is located are collected. (Figure 5-6). The basin was found in the modeled basin and the basin was found to feed the downstream point of the Karpuz Stream (Figure 7).

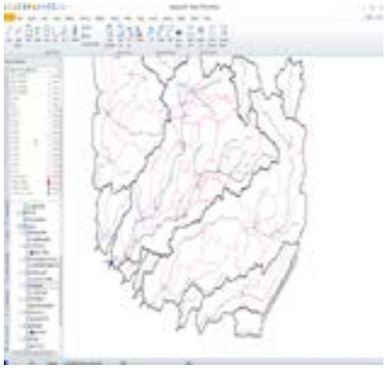

Figure 5. Basin areas and flow lines resulting from modeling of basins

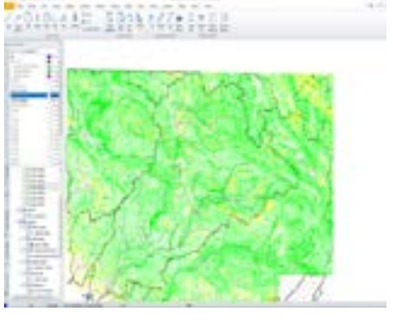

Figure 6. Upper Basin of the Working Area

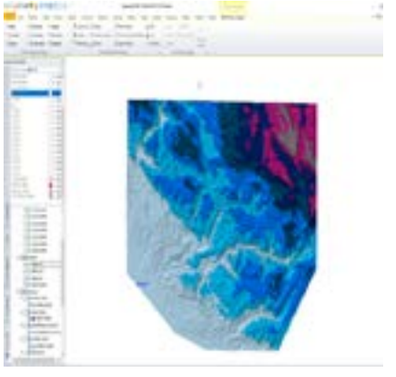

Figure 7. Modeling of Project Area Basins

Mockus, DSI synthetic methods and Regional flood frequency analysis for flood flow calculation

If there is sufficient flow data in a river basin, statistical methods give accurate results in the calculation of flood flow rates. However, generally, there is no precipitation - flow data that can form a unit hydrograph in rainfall areas. In these cases, synthetic unit hydrographs are used.

Mockus Method

When working with the Mockus method, first Tc collection time, D downtime and Tp peak flow time parameters should be determined. These terms are calculated by the equations given below[1]. (Equations 1, 2 and 3).

$$Tc = 0{,}00032\ (L^{0{,}77} * S^{0{,}385})$$

$$D = 2 * \sqrt{T_c}$$

$$Tp = 0{,}5 * D + 0{,}6 * Tc$$

DSI Synthetic Method

DSI in the synthetic method, a flow rate (q, lt / sec / mm / km^2) which will be taken from the unit area of a 2 hour precipitation period should be calculated [14]. The materials required for the DSI synthetic unit hydrograph method were obtained during the modeling phase of the basins. Formulas for unit hydrograph calculations are given in (Equations 4, 5, 6, 7 and 8) [4].

$$q_p = \frac{414}{A^{0{,}225}\left(L * \frac{L}{S^{0{,}5}}\right)^{0{,}16}}$$

(1mm flow for rain efficiency) (4)

$$Q_p = A^{*}q_p{}^{*}10^{-3}$$ (peak flow rate) (5)

$$V_b = A^{*}10^{3}$$ (unit hydrograph volume) (6)

$$T = 3{,}65^{*}V_b/Q_b$$ *(duration of hydrograph)* (7)

$$T_p = T/5$$

(duration of hydrograph peak flow rate) (8)

Regional flood frequency analysis

In the basins without sufficient number or no flow observation stations, it is the method where the calculations are made by using the flow observation stations in the nearby basins to determine the flow rates of the floods [12]. This method consist of parts;

- decide the probability distributions of stations
- determine the homogeneity of the stations in the basin
- determine the ratio of T-year flood(Q_t) flows to 2-year flow rate (Q_2)
- derivation of the regional dimensionless flood frequency curves following(Figure 9)

- Regression relationship between Q_2 and drainage area [18].

RESULTS AND DISCUSSIONS

Calculation of spatial distributions and precipitation values of point precipitation data

Precipitation stations are used as input data for flood flow accounts. The spatial distribution of this pointy precipitation data on the basin was calculated (Figure 8). Thiessen polygons were used to calculate the spatial distributions on the basin determined by the downstream point.

According to the Thiessen Polygon, the rainfall area is represented by 72% Manavgat MS and 28% Alanya MS. Normal distribution, Log-Normal (2 parameters), Log-Normal (3 parameters), Pearson Type3 (Gamma Type 3), Log Pearson Type3 and Gumbel methods were used to calculate the total rainfall data of each station on the polygon area of the basin.

Figure 8. Spatial distribution of precipitation stations on basin area

The maximum rainfall of the meteorological stations in the project and the appropriate distribution according to the Kolmogorov Smirnov test are given in Tables 2 and 3.

Tablo 2. Maximum rainfall and suitable distribution of Alanya meteorological station

ALANYA METEOROLOGY STATION DISTRIBUTION OF DAILY MAXIMUM PRECIPITATION									
Type	2	5	10	25	50	100	200	500	Accepted
Normal Distribution	97.5	126.8	142.1	158.5	169.0	178.5	187.1	197.6	
Log-Normal 2	91.9	122.9	143.2	168.4	187.0	205.5	223.9	248.4	
Log-Normal 3	91.5	122.5	143.0	168.9	188.2	207.6	227.1	253.1	
Pearson Type-3	90.5	122.8	144.1	170.5	189.6	208.2	226.4	244.6	
Log-Pearson Type-3	91.4	122.0	142.5	168.8	188.7	208.9	229.5	252.1	***
Gumbel	92.1	125.6	147.8	175.8	196.6	217.3	237.9	265.0	

STATISTICS PARAMETERS	
Year Number	61
Linear Skewness	1.251
Logarithmic Skewness	0.000
Linear Mean	97.549
Linear St.Deviation	34.786
Logarithmic Mean	1.965
Logarithmic St. Deviation	0.146

RESULTS OF DISTRIBUTION TYPES ACCORDING TO SIMIMNOV-KOLMOGOROV TEST									
Type	Theoric	Empirical	Maximum	Observation	Significance Percentages				
	P	P	P Dmax	Value P	0.80	0.85	0.90	0.95	0.99
Normal Distribution	0.51	0.66	**0.16**	98.00	Reject	Reject	Accept	Accept	Accept
Log-Normal 2	0.79	0.11	**0.10**	69.60	Accept	Accept	Accept	Accept	Accept
Log-Normal 3	0.79	0.11	**0.10**	69.60	Accept	Accept	Accept	Accept	Accept
Pearson Type-3	0.22	0.11	**0.10**	69.60	Accept	Accept	Accept	Accept	Accept
Log-Pearson Type-3	0.20	0.11	**0.09**	69.60	Accept	Accept	Accept	Accept	Accept
Gumbel	0.23	0.11	**0.11**	69.60	Accept	Accept	Accept	Accept	Accept

Table 3. Maximum rainfall and suitable distribution of Manavgat meteorological station

MANAVGAT METEOROLOGY STATION DISTRIBUTION OF DAILY MAXIMUM PRECIPITATION									
Tipi	2	5	10	25	50	100	200	500	Accepted
Normal Distribution	105.2	135.1	150.6	167.3	178.0	187.6	196.4	207.1	
Log-Normal 2	99.8	131.4	151.8	177.0	195.5	213.7	231.8	255.8	
Log-Normal 3	99.5	131.1	151.7	177.4	196.3	215.1	233.8	258.7	
Pearson Type-3	98.6	131.4	152.7	178.7	197.4	215.5	233.2	250.8	
Log-Pearson Type-3	97.4	128.6	151.0	181.7	206.2	232.2	259.9	290.9	***
Gumbel	99.7	134.0	156.7	185.4	206.7	227.9	248.9	276.7	

STATISTICS PARAMETERS	
Year Number	56
Linear Skewness	1.142716
Logarithmic Skewness	0
Linear Mean	105.2464
Linear St.Deviation	35.41651
Logarithmic Mean	2.000717
Logarithmic St. Deviation	0.134631

RESULTS OF DISTRIBUTION TYPES ACCORDING TO SIMIMNOV-KOLMOGOROV TEST									
Type	Theoric	Empirical	Maximum	Observation	Significance Percentages				
	P	P	P Dmax	Value P	0.80	0.85	0.90	0.95	0.99
Normal Distribution	0.52	0.67	**0.15**	106.80	Reject	Accept	Accept	Accept	Accept
Log-Normal 2	0.66	0.42	**0.09**	86.80	Accept	Accept	Accept	Accept	Accept
Log-Normal 3	0.66	0.42	**0.08**	86.80	Accept	Accept	Accept	Accept	Accept
Pearson Type-3	0.57	0.67	**0.09**	106.80	Accept	Accept	Accept	Accept	Accept
Log-Pearson Type-3	0.60	0.67	**0.07**	106.80	Accept	Accept	Accept	Accept	Accept
Gumbel	0.58	0.67	**0.09**	106.80	Accept	Accept	Accept	Accept	Accept

The rainfall area of the project site is determined according to the percentages of meteorological stations affecting the average and given in Table 4.

Table 4. Precipitation analysis of precipitation stations

Station Name	Thissen Percentages (%)	2	5	10	25	50	100	500
Manavgat MS	0.72	97.4	128.6	151.0	181.7	206.2	232.2	290.9
Alanya MS	0.28	91.4	122.0	142.5	168.8	188.7	208.9	252.1
Rainfall Area Mean	**1.00**	**95.8**	**126.7**	**148.7**	**178.1**	**201.3**	**225.7**	**280.0**

Characteristic information about the Karpuz Stream basin was obtained by modeling (Table 5,6 and 7).

Mockus Method

T_c collection time, D downtime and T_p peak flow time parameters given below.

Tablo 5. Characteristics and Harmonic Slope

A(km²)	L(km)	L_c(km)	$S_{Har.}$
622.80	58.60	34.00	0.015

Number	Elevation (m)	Elevation Difference (m)	L/10 (m)	(l/h)^0.5
0	4			
1	26	22	5860	16.321
2	76	50	5860	10.826
3	123	47	5860	11.166
4	185	62	5860	9.722
5	304	119	5860	7.017
6	413	109	5860	7.332
7	521	108	5860	7.366
8	700	179	5860	5.722
9	1213	513	5860	3.380
10	2450	1237	5860	2.177
			TOTAL	**81.03**

Table 6. Basin Precipitation Correction Factors in Critical Precipitation Times in Project Location

Critical Precipitation Times (sa)	0.5	1	2	3	4	5	6	8	12	18	24
Cor..Plv.Perc.(Manavgat)	0.27	0.36	0.46	0.51	0.56	0.60	0.64	0.70	0.81	0.92	1.00
Precipitation-Area-Distribution Percentage	0.55	0.66	0.72	0.79	0.80	0.82	0.84	0.85	0.86	0.89	0.91
Maximize factor MF	1.13	1.13	1.13	1.13	1.13	1.13	1.13	1.13	1.13	1.13	1.13

Table 7. Project Location Flow Curve Number Determination

Basin Status	Area (%)	Curve Number	Area (%)*Curve Number
Mountainous Bare Area (Infiltration-Soil Group-D)	12	84	1008
Residential Area (Soil Group-C)	3	82	246
Agricultural Area (Infiltration Good-Land Group) B	5	70	350
Forest Area (Leakage Good-Soil Group-B)	12	55	660
Woodland (Infiltrate Weak-Earth Group-B	39	66	2574
Woodland (Infiltration-Earth Group-B	29	60	1740
Total	100		6508

After the determination of these parameters, the repetitive flow calculations are performed (Table 8).

Table 8. Mockus Method Flood Flow Calculations

	T(Sa)	MF	PADP	PLV		
	5.5	1.13	0.835	0.620		
	Tc(sa)	D	Tp			
	7.52	5.48	7.260			
	RAİNFALL AREA 24 HOURS REPLACEMENT VALUES (mm)					
	2	5	10	25	50	100
LAST CHARGE	95.75	126.71	148.65	178.10	201.31	225.69
0.585001	73.06	95.70	109.37	125.55	136.94	147.86
FLOW (mm)	11.45	22.77	30.75	41.04	48.74	56.44
FLOOD FLOW (m^3/s)	**221.78**	**423.87**	**566.12**	**749.75**	**887.23**	**1024.60**

DSI Synthetic Method

Flood flow rates were determined according to the DSI method(Table 9).

Table 9. DSI Synthetic Method of Flood Flow Calculation

qp(L/s/km²/mm)	Qp(m³/s/mm)	Vb(m3)	T(sa)	Tp(sa)			
20.653	12.863	622800	49	10			
PROJECT DOWNPOUR TİMES						Unit:m^3/s	
Flow	2	4	6	8	12	18	24
Q_2	49.7	113.6	173.7	210.2	273.9	315.9	**336.3**
Q_5	106.4	222.3	321.1	377.6	471.0	524.4	**549.9**
Q_{10}	150.9	301.0	424.6	492.8	603.5	665.2	**690.9**
Q_{25}	211.9	404.4	557.7	640.9	770.3	840.7	**866.6**
Q_{50}	259.4	482.7	657.1	750.8	893.6	970.1	**996.5**
Q_{100}	308.2	561.4	756.4	860.0	1015.3	1097.3	**1125.0**

Regional flood frequency analysis

Regional flood frequency analyses including homogeneity test was applied to annual instantaneous peak flows of seven flow gauging station(FGS) (Table 10).

Table10. Regional Flood Frequency Analysis of Flow Gauging Stations

Number	Station No	N (Year)	A (Km^2)	Q_2	Q_5	Q_{10}	Q_{25}	Q_{50}	Q_{100}
1	D09A067	39	303.2	122.7	178.8	217.7	268.7	307.7	347.6
2	D09A068	29	336.3	181.5	290.8	364.5	459.3	530.6	602.8
3	D09A084	28	46.0	42.9	77.6	103.1	136.3	161.2	186.0
4	E09A020	30	438.0	269.4	365.9	436.4	533.2	611.2	694.3
5	E09A917	50	863.0	363.4	622.9	826.8	1119.2	1361.7	1624.7
6	D09A013	48	195.0	221.8	390.5	511.6	669.9	789.5	908.7
7	D17A038	21	158.0	98.2	168.2	217.7	277.9	320.9	362.5

After that derivation of the regional dimensionless flood frequency curves following given below(Figure 9).

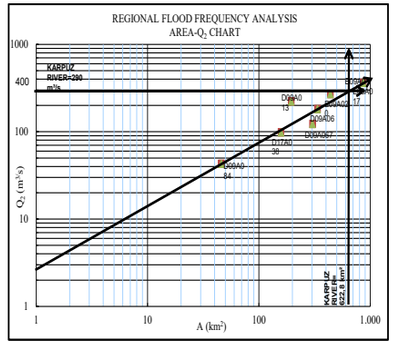

Figure 9. Regional Flood Frequency Analysis Area-Q2 Chart

CONCLUSION

In this study, Antalya Karpuz Stream was modeled in accordance with Taudem algorithm to main and lower basins. Flow lines in each basin, flow directions of these arms and rainfall areas and harmonic slopes were determined according to these directions. In addition to these parameters determined for the Karpuz Stream, the meteorological stations affecting the basin were determined and the rainfall analysis was performed with the daily total precipitation values of these stations. For the determination of 24-hour recurrent precipitation values, the spatial distributions of the point rainfall data were determined according to the Thiessen method and the precipitation values for the basin were calculated. According to DSI synthetic, Mockus methods and Regional Frequency Analysis, flood flow calculations are done and the results are given in Table 11 and comparative columns are given in Figure 10.

Table 11. Comparative Flood Flow Calculation

Karpuz Stream Comparative Flood Flow Calculation			
	DSI synthetic	Mockus	RFA
Q_2	336.3	221.78	290.0
Q_5	549.9	423.87	481.1
Q_{10}	690.9	566.12	619.3
Q_{25}	866.6	749.75	808.8
Q_{50}	996.5	887.23	939.8
Q_{100}	1125.0	1024.60	1081.8

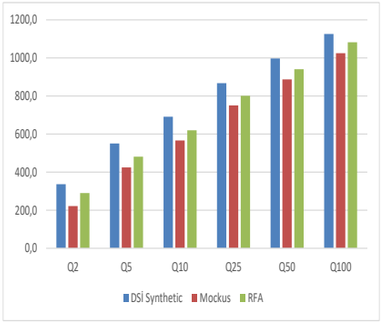

Figure 10. Karpuz Stream Comparative Recursive Flow Chart

As a result of the comparisons, it was seen that the DSI Synthetic method, where the increment flows were calculated, gave greater flow values than the Mockus method and Regional Frequency Analysis.

REFERENCES

1. Aslan, B. S.C.S. Applicable Investigation in Turkey Terms of Synthetic Unit Hydrograph Method, ITU, Institute of Science and Technology, MSc, Istanbul Technical University, İstanbul,Turkey,1997.

2. Bayazıt, M. Hydrological models, Istanbul Technical University Faculty of Civil Engineering, Istanbul, Turkey, 1998.

3. Camarasa, A.M., Tilford, K.A. Rainfall-Runoff Modelling of Ephemeral Streams in the Valencia Region (Eastern Spain). Hydrological Processes, 16, pp. 3329-3344, 2002.

4. Cetiner, H.İ. Modeling of Ergene Basin with Computer Software According to Taudem Algorithm and Comparison of Results by Calculating Flood Flow Rates of Ova River According to DSİ Synthetic and Mockus Methods, 4th International Water Congress, 2-4 November 2017, Water in Smart Cities Management, pp. 226-235, Izmir, Turkey, 2017.

5. Gunal, A.Y., Guven, A. Synthetic Unit Hydrograph of Small Catchments by Using GIS. Acta Physica Polonica Series, 130, pp.130-132, 2016.

6. Gurkan, D. Investigation of the Effects of Climate Changes on Surface Water Resources in Seyhan Basin, Hacettepe University International Karst Water Resources Application and Research Center, Ankara. Unpublished Master Thesis. Hacettepe University, Institute of Science, Geological Engineering Department, 2016.

7. Jennings, S. , Elsaesser, B. , Baker, G. , Bree, T. , Daly, D. , Fitzpatrick, J., Glasgow, Hunter-Williams, T. An Integrated Approach to Quantifying Groundwater and Surface Water Contributions of Stream Flow, Hydrology Ireland, 2003.

8. Khandan, N.N. Modelling tools for environmental engineers and scientists, CRC Press LLC, 2000 N.W. Corporate Blvd., Boca Raton, Florida, 2002.

9. Ozbayrak, E., Bakan, G. The Concept of Environmental Model and Classifications, 6. National Environmental Engineering Congress, 24-25-26 November 2005, Istanbul, Turkey, 2005.

10. Ozdemir, H. Applied Flood Hydrology. DSİ Printing and Photo-Film Operation Directorate Printing House, 81-94, Ankara, Turkey, 1978.

11. Saplıoğlu, K. Flow Prediction with Parametric Basin Modeling: Kopruçay River Basin. PhD Thesis, Suleyman Demirel University, Institute of Science and Civil Engineering, 198, Isparta, Turkey, 2010.

12. Seckin, N. Flood Frequency Analysis of Ceyhan and Seyhan Basins, MSc, Cukurova University, Institute of Science, Civil Engineering Department, 132.Adana, Turkey, 2002.

13. Sarlak, N., Tigrek. S. Point Flood Frequency Analysis: Göksu River and Kayraktepe Dam Case Analysis, Journal of the Faculty of Engineering and Architecture of Gazi University, 31: 4, pp. 1095-1103, 2016.

14. Sonmez, O., Hırca, F., Demir, F. Recurring Flood Flow Rate Calculation with Different Precipitation Flow Models in Rivers without Flow Measurement: The Case of Mudurnu Çayı, 5th International Symposium on Innovative Technologies in Engineering and Science 29-30 September 2017, ISITES2017 Baku, Azerbaijan, 2017.

15. Sen, Z. In Hydrology; Data Processing, Interpretation and Design. Symposium Notes, Water Foundation Publications, Istanbul, Turkey, 2002.

16. Tarboton, D. A New Method for the Determination of Flow Directions and Upslope Areas in Grid Digital Elevation Models. Water Resources Research, 33, pp. 309-319, 1997.

17. Tayfur, G., Singh, V., P. ANN and fuzzy logic models for simulating event based rainfall-runoff. Journal of hydraulic engineering, ASCE, 132(12), pp. 1321-1330, 2006.

18. Topaloglu, F. Regional Flood Frequency Analysis of the Basins of the East Mediterranean Region. Turkish Journal of Agriculture and Forestry, 29, pp. 287-295, 2005.

19. Zoppou, C. Review of storm water models, CSIRO land and water technical report, 52/99, Canberra, Australia, 1999.